

CHAPTER 7: Fixed-Bed Catalytic Reactors I

Copyright © 2025 by Nob Hill Publishing, LLC

- In a fixed-bed reactor the catalyst pellets are held in place and do not move with respect to a fixed reference frame.
- Material and energy balances are required for both the fluid, which occupies the interstitial region between catalyst particles, and the catalyst particles, in which the reactions occur.
- The following figure presents several views of the fixed-bed reactor. The species production rates in the bulk fluid are *essentially zero*. That is the reason we are using a catalyst.

CHAPTER 7: Fixed-Bed Catalytic Reactors II

Copyright © 2025 by Nob Hill Publishing, LLC

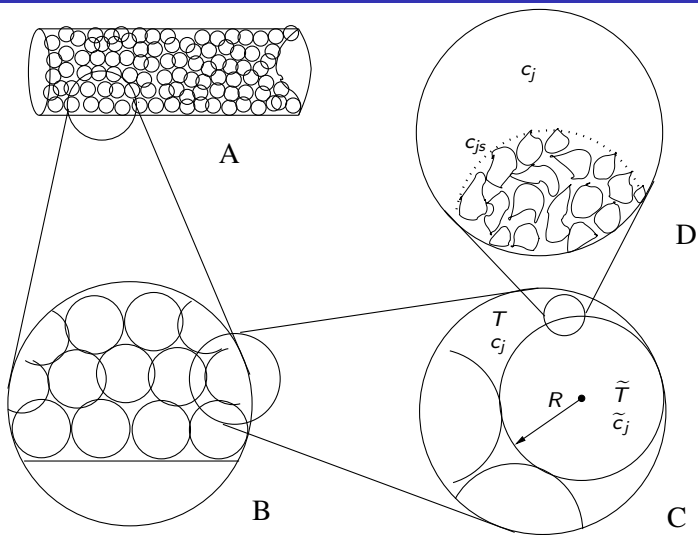


Figure 7.1: Expanded views of a fixed-bed reactor.

- Essentially all reaction occurs within the catalyst particles. The fluid in contact with the external surface of the catalyst pellet is denoted with subscript s .
- When we need to discuss both fluid and pellet concentrations and temperatures, we use a tilde on the variables within the catalyst pellet.

The steps to consider

During any catalytic reaction the following steps occur:

- 1 transport of reactants and energy from the bulk fluid up to the catalyst pellet exterior surface,
- 2 transport of reactants and energy from the external surface into the porous pellet,
- 3 adsorption, chemical reaction, and desorption of products at the catalytic sites,
- 4 transport of products from the catalyst interior to the external surface of the pellet, and
- 5 transport of products into the bulk fluid.

The coupling of transport processes with chemical reaction can lead to concentration and temperature gradients within the pellet, between the surface and the bulk, or both.

- Usually one or at most two of the five steps are rate limiting and act to influence the overall rate of reaction in the pellet. The other steps are inherently faster than the slow step(s) and can accommodate any change in the rate of the slow step.
- The system is *intraparticle transport controlled* if step 2 is the slow process (sometimes referred to as diffusion limited).
- For *kinetic or reaction control*, step 3 is the slowest process.
- Finally, if step 1 is the slowest process, the reaction is said to be *externally transport controlled*.

- In this chapter, we model the system on the scale of Figure 7.1 C. The problem is solved for one pellet by averaging the microscopic processes that occur on the scale of level D over the volume of the pellet or over a solid surface volume element.
- This procedure requires an effective diffusion coefficient, D_j , to be identified that contains information about the physical diffusion process and pore structure.

- To make a catalytic process commercially viable, the number of sites per unit reactor volume should be such that the rate of product formation is on the order of 1 mol/L·hour [12].
- In the case of metal catalysts, the metal is generally dispersed onto a high-area oxide such as alumina. Metal oxides also can be dispersed on a second carrier oxide such as vanadia supported on titania, or it can be made into a high-area oxide.
- These carrier oxides can have surface areas ranging from 0.05 m²/g to greater than 100 m²/g.
- The carrier oxides generally are pressed into shapes or extruded into pellets.

- The following shapes are frequently used in applications:
 - 20–100 μm diameter spheres for fluidized-bed reactors
 - 0.3–0.7 cm diameter spheres for fixed-bed reactors
 - 0.3–1.3 cm diameter cylinders with a length-to-diameter ratio of 3–4
 - up to 2.5 cm diameter hollow cylinders or rings.
- Table 7.1 lists some of the important commercial catalysts and their uses [7].

Catalyst	Reaction
Metals (e.g., Ni, Pd, Pt, as powders or on supports) or metal oxides (e.g., Cr ₂ O ₃)	C=C bond hydrogenation, e.g., olefin + H ₂ → paraffin
Metals (e.g., Cu, Ni, Pt)	C=O bond hydrogenation, e.g., acetone + H ₂ → isopropanol
Metal (e.g., Pd, Pt)	Complete oxidation of hydrocarbons, oxidation of CO
Fe (supported and promoted with alkali metals)	3H ₂ + N ₂ → 2NH ₃
Ni	CO + 3H ₂ → CH ₄ + H ₂ O (methanation)
Fe or Co (supported and promoted with alkali metals)	CO + H ₂ → paraffins + olefins + H ₂ O + CO ₂ (+ other oxygen-containing organic compounds) (Fischer-Tropsch reaction)
Cu (supported on ZnO, with other components, e.g., Al ₂ O ₃)	CO + 2H ₂ → CH ₃ OH
Re + Pt (supported on η-Al ₂ O ₃ or γ-Al ₂ O ₃ promoted with chloride)	Paraffin dehydrogenation, isomerization and dehydrocyclization

Catalyst	Reaction
Solid acids (e.g., $\text{SiO}_2\text{-Al}_2\text{O}_3$, zeolites)	Paraffin cracking and isomerization
$\gamma\text{-Al}_2\text{O}_3$	Alcohol \rightarrow olefin + H_2O
Pd supported on acidic zeolite	Paraffin hydrocracking
Metal-oxide-supported complexes of Cr, Ti or Zr	Olefin polymerization, e.g., ethylene \rightarrow polyethylene
Metal-oxide-supported oxides of W or Re	Olefin metathesis, e.g., 2 propylene \rightarrow ethylene + butene
Ag(on inert support, promoted by alkali metals)	Ethylene + $1/2 \text{O}_2 \rightarrow$ ethylene oxide (with $\text{CO}_2 + \text{H}_2\text{O}$)
V_2O_5 or Pt	$2 \text{SO}_2 + \text{O}_2 \rightarrow 2 \text{SO}_3$
V_2O_5 (on metal oxide support)	Naphthalene + $9/2 \text{O}_2 \rightarrow$ phthalic anhydride + $2\text{CO}_2 + 2\text{H}_2\text{O}$
Bismuth molybdate	Propylene + $1/2 \text{O}_2 \rightarrow$ acrolein
Mixed oxides of Fe and Mo	$\text{CH}_3\text{OH} + \text{O}_2 \rightarrow$ formaldehyde (with $\text{CO}_2 + \text{H}_2\text{O}$)
Fe_3O_4 or metal sulfides	$\text{H}_2\text{O} + \text{CO} \rightarrow \text{H}_2 + \text{CO}_2$

Table 7.1: Industrial reactions over heterogeneous catalysts. This material is used by permission of John Wiley & Sons, Inc., Copyright ©1992 [7].

- Figure 7.1 D of shows a schematic representation of the cross section of a single pellet.
- The solid density is denoted ρ_s .
- The pellet volume consists of both void and solid. The pellet void fraction (or porosity) is denoted by ϵ and

$$\epsilon = \rho_p V_g$$

in which ρ_p is the effective particle or pellet density and V_g is the pore volume.

- The pore structure is a strong function of the preparation method, and catalysts can have pore volumes (V_g) ranging from 0.1–1 cm³/g pellet.

- The pores can be the same size or there can be a bimodal distribution with pores of two different sizes, a large size to facilitate transport and a small size to contain the active catalyst sites.
- Pore sizes can be as small as molecular dimensions (several Ångströms) or as large as several millimeters.
- Total catalyst area is generally determined using a physically adsorbed species, such as N_2 . The procedure was developed in the 1930s by Brunauer, Emmett and Teller [5], and the isotherm they developed is referred to as the BET isotherm.

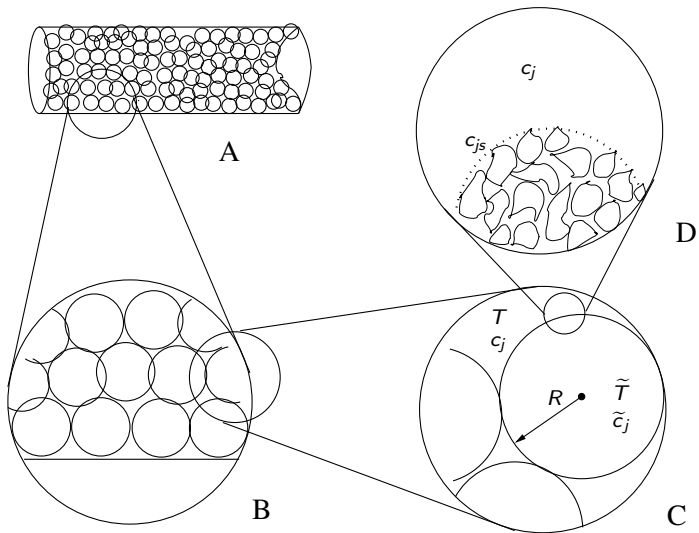


Figure: Expanded views of a fixed-bed reactor.

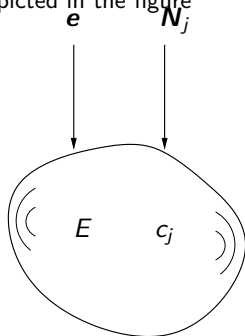
Catalyst	ϵ	τ
100–110 μm powder packed into a tube	0.416	1.56
pelletized Cr_2O_3 supported on Al_2O_3	0.22	2.5
pelletized boehmite alumina	0.34	2.7
Girdler G-58 Pd on alumina	0.39	2.8
Haldor-Topsøe MeOH synthesis catalyst	0.43	3.3
0.5% Pd on alumina	0.59	3.9
1.0% Pd on alumina	0.5	7.5
pelletized Ag/8.5% Ca alloy	0.3	6.0
pelletized Ag	0.3	10.0

Table 7.2: Porosity and tortuosity factors for diffusion in catalysts.

The General Balances in the Catalyst Particle

In this section we consider the mass and energy balances that arise with diffusion in the solid catalyst particle when considered at the scale of Figure 7.1 C.

Consider the volume element depicted in the figure



Assume a fixed laboratory coordinate system in which the velocities are defined and let \mathbf{v}_j be the velocity of species j giving rise to molar flux \mathbf{N}_j

$$\mathbf{N}_j = c_j \mathbf{v}_j, \quad j = 1, 2, \dots, n_s$$

Let E be the total energy within the volume element and \mathbf{e} be the flux of total energy through the bounding surface due to all mechanisms of transport. The conservation of mass and energy for the volume element implies

$$\begin{aligned} \frac{\partial c_j}{\partial t} &= -\nabla \cdot \mathbf{N}_j + R_j, & j = 1, 2, \dots, n_s \\ \frac{\partial E}{\partial t} &= -\nabla \cdot \mathbf{e} \end{aligned} \quad (7.10)$$

in which R_j accounts for the production of species j due to chemical reaction.

Next we consider the fluxes. Since we are considering the diffusion of mass in a stationary, solid particle, we assume the mass flux is well approximated by

$$\mathbf{N}_j = -D_j \nabla c_j, \quad j = 1, 2, \dots, n_s$$

in which D_j is an effective diffusivity for species j . We approximate the total energy flux by

$$\mathbf{e} = -\hat{k} \nabla T + \sum_j \mathbf{N}_j \bar{H}_j$$

This expression accounts for the transfer of heat by conduction, in which \hat{k} is the effective thermal conductivity of the solid, and transport of energy due to the mass diffusion.

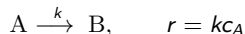
In this chapter, we are concerned mostly with the steady state. Setting the time derivatives to zero and assuming constant thermodynamic properties produces

$$0 = D_j \nabla^2 c_j + R_j, \quad j = 1, 2, \dots, n_s \quad (7.14)$$

$$0 = \hat{k} \nabla^2 T - \sum_i \Delta H_{Ri} r_i \quad (7.15)$$

In multiple-reaction, nonisothermal problems, we must solve these equations numerically, so the assumption of constant transport and thermodynamic properties is driven by the lack of data, and not analytical convenience.

- We start with the simplest cases and steadily remove restrictions and increase the generality. We consider in this section a single reaction taking place in an *isothermal* particle.
- First case: the spherical particle, first-order reaction, without external mass-transfer resistance.
- Next we consider other catalyst shapes, then other reaction orders, and then other kinetic expressions such as the Hougen-Watson kinetics of Chapter 5.
- We end the section by considering the effects of finite external mass transfer.



$$0 = D_j \nabla^2 c_j + R_j, \quad j = 1, 2, \dots, n_s$$

Substituting the production rate into the mass balance, expressing the equation in spherical coordinates, and assuming pellet symmetry in θ and ϕ coordinates gives

$$D_A \frac{1}{r^2} \frac{d}{dr} \left(r^2 \frac{dc_A}{dr} \right) - kc_A = 0 \quad (7.16)$$

in which D_A is the effective diffusivity in the pellet for species A.

As written here, the first-order rate constant k has units of inverse time.

Be aware that the units for a heterogeneous reaction rate constant are sometimes expressed per mass or per area of catalyst.

In these cases, the reaction rate expression includes the conversion factors, catalyst density or catalyst area, as illustrated in Example 7.1.

- We require *two* boundary conditions for Equation 7.16.
- In this section we assume the concentration at the outer boundary of the pellet, c_{As} , is known
- The symmetry of the spherical pellet implies the vanishing of the derivative at the center of the pellet.
- Therefore the two boundary conditions for Equation 7.16 are

$$\begin{aligned}c_A &= c_{As}, & r &= R \\ \frac{dc_A}{dr} &= 0 & r &= 0\end{aligned}$$

Dimensionless form I

At this point we can obtain better insight by converting the problem into dimensionless form. Equation 7.16 has two dimensional quantities, length and concentration. We might naturally choose the sphere radius R as the length scale, but we will find that a better choice is to use the pellet's volume-to-surface ratio. For the sphere, this characteristic length is

$$a = \frac{V_p}{S_p} = \frac{\frac{4}{3}\pi R^3}{4\pi R^2} = \frac{R}{3}$$

The only concentration appearing in the problem is the surface concentration in the boundary condition, so we use that quantity to nondimensionalize the concentration

$$\bar{r} = \frac{r}{a}, \quad \bar{c} = \frac{c_A}{c_{As}}$$

Dividing through by the various dimensional quantities produces

$$\frac{1}{\bar{r}^2} \frac{d}{d\bar{r}} \left(\bar{r}^2 \frac{d\bar{c}}{d\bar{r}} \right) - \Phi^2 \bar{c} = 0 \quad (7.17)$$

$$\bar{c} = 1 \quad \bar{r} = 3$$

$$\frac{d\bar{c}}{d\bar{r}} = 0 \quad \bar{r} = 0$$

in which Φ is given by

$$\Phi = \sqrt{\frac{ka^2}{D_A}} \quad \frac{\text{reaction rate}}{\text{diffusion rate}} \quad \text{Thiele modulus}$$

(7.18)

The single dimensionless group appearing in the model is referred to as the Thiele number or Thiele modulus in recognition of Thiele's pioneering contribution in this area [11].¹ The Thiele modulus quantifies the ratio of the reaction rate to the diffusion rate in the pellet.

¹In his original paper, Thiele used the term *modulus* to emphasize that this then unnamed dimensionless group was positive. Later when Thiele's name was assigned to this dimensionless group, the term modulus was retained. Thiele number would seem a better choice, but the term Thiele modulus has become entrenched.

We now wish to solve Equation 7.17 with the given boundary conditions. Because the reaction is first order, the model is linear and we can derive an analytical solution. It is often convenient in spherical coordinates to consider the variable transformation

$$\bar{c}(\bar{r}) = \frac{u(\bar{r})}{\bar{r}} \quad (7.20)$$

Substituting this relation into Equation 7.17 provides a simpler differential equation for $u(\bar{r})$,

$$\frac{d^2 u}{d\bar{r}^2} - \Phi^2 u = 0 \quad (7.21)$$

with the transformed boundary conditions

$$\begin{aligned} u &= 3 & \bar{r} &= 3 \\ u &= 0 & \bar{r} &= 0 \end{aligned}$$

The boundary condition $u = 0$ at $\bar{r} = 0$ ensures that \bar{c} is finite at the center of the pellet.

The solution to Equation 7.21 is

$$u(\bar{r}) = c_1 \cosh \Phi \bar{r} + c_2 \sinh \Phi \bar{r} \quad (7.22)$$

This solution is analogous to the sine and cosine solutions if one replaces the negative sign with a positive sign in Equation 7.21. These functions are shown in Figure 7.3.

General solution – hyperbolic functions II

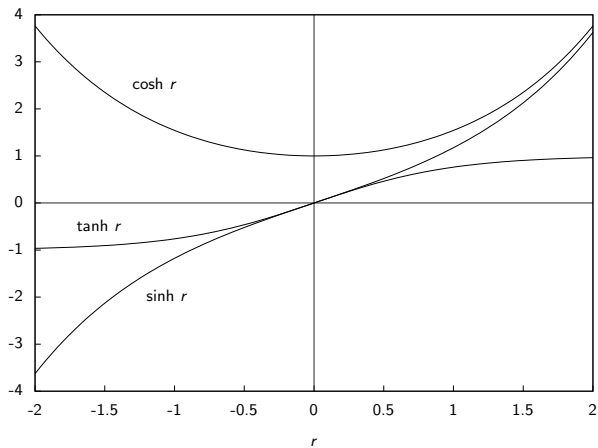


Figure 7.3: Hyperbolic trigonometric functions \sinh , \cosh and \tanh .

Some of the properties of the hyperbolic functions are

$$\cosh r = \frac{e^r + e^{-r}}{2} \quad \frac{d \cosh r}{dr} = \sinh r$$

$$\sinh r = \frac{e^r - e^{-r}}{2} \quad \frac{d \sinh r}{dr} = \cosh r$$

$$\tanh r = \frac{\sinh r}{\cosh r}$$

The constants c_1 and c_2 are determined by the boundary conditions. Substituting Equation 7.22 into the boundary condition at $\bar{r} = 0$ gives $c_1 = 0$, and applying the boundary condition at $\bar{r} = 3$ gives $c_2 = 3/\sinh 3\Phi$.

Substituting these results into Equations 7.22 and 7.20 gives the solution to the model

$$\bar{c}(\bar{r}) = \frac{3 \sinh \Phi \bar{r}}{\bar{r} \sinh 3\Phi} \quad (7.23)$$

Figure 7.4 displays this solution for various values of the Thiele modulus. Note for small values of Thiele modulus, the reaction rate is small compared to the diffusion rate, and the pellet concentration becomes nearly uniform. For large values of Thiele modulus, the reaction rate is large compared to the diffusion rate, and the reactant is converted to product before it can penetrate very far into the pellet.

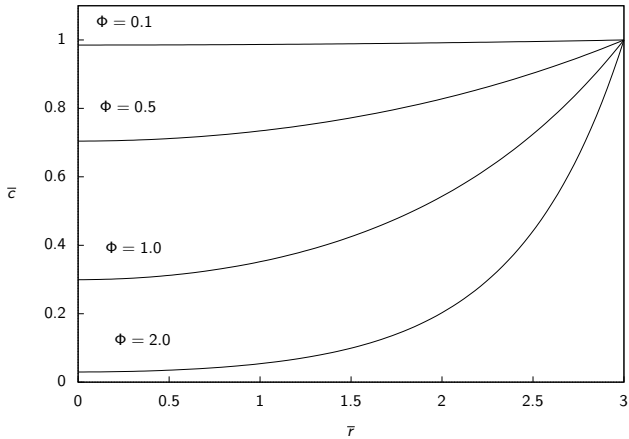


Figure 7.4: Dimensionless concentration versus dimensionless radial position for different values of the Thiele modulus.

We now calculate the pellet's overall production rate given this concentration profile. We can perform this calculation in two ways.

The first and more direct method is to integrate the local production rate over the pellet volume. The second method is to use the fact that, at steady state, the rate of consumption of reactant within the pellet is equal to the rate at which material fluxes through the pellet's exterior surface.

The two expressions are

$$R_{Ap} = \frac{1}{V_p} \int_0^R R_A(r) 4\pi r^2 dr \quad \text{volume integral} \quad (7.24)$$

$$R_{Ap} = -\frac{S_p}{V_p} D_A \left. \frac{dc_A}{dr} \right|_{r=R} \quad \begin{array}{l} \text{surface flux} \\ \text{(assumes steady state)} \end{array} \quad (7.25)$$

in which the local production rate is given by $R_A(r) = -kc_A(r)$.

We use the direct method here and leave the other method as an exercise.

Substituting the local production rate into Equation 7.24 and converting the integral to dimensionless radius gives

$$R_{Ap} = -\frac{kC_{As}}{9} \int_0^3 \bar{c}(\bar{r}) \bar{r}^2 d\bar{r}$$

Substituting the concentration profile, Equation 7.23, and changing the variable of integration to $x = \Phi r$ gives

$$R_{Ap} = -\frac{kC_{As}}{3\Phi^2 \sinh 3\Phi} \int_0^{3\Phi} x \sinh x dx$$

The integral can be found in a table or derived by integration by parts to yield finally

$$R_{Ap} = -kC_{As} \frac{1}{\Phi} \left[\frac{1}{\tanh 3\Phi} - \frac{1}{3\Phi} \right] \quad (7.26)$$

It is instructive to compare this actual pellet production rate to the rate in the absence of diffusional resistance. If the diffusion were arbitrarily fast, the concentration everywhere in the pellet would be equal to the surface concentration, corresponding to the limit $\Phi = 0$. The pellet rate for this limiting case is simply

$$R_{As} = -kC_{As} \quad (7.27)$$

We define the effectiveness factor, η , to be the ratio of these two rates

$$\eta \equiv \frac{R_{Ap}}{R_{As}}, \quad \text{effectiveness factor} \quad (7.28)$$

The effectiveness factor is a dimensionless pellet production rate that measures how effectively the catalyst is being used.

For η near unity, the entire volume of the pellet is reacting at the same high rate because the reactant is able to diffuse quickly through the pellet.

For η near zero, the pellet reacts at a low rate. The reactant is unable to penetrate significantly into the interior of the pellet and the reaction rate is small in a large portion of the pellet volume.

The pellet's diffusional resistance is large and this resistance lowers the overall reaction rate.

We can substitute Equations 7.26 and 7.27 into the definition of effectiveness factor to obtain for the first-order reaction in the spherical pellet

$$\eta = \frac{1}{\Phi} \left[\frac{1}{\tanh 3\Phi} - \frac{1}{3\Phi} \right] \quad (7.29)$$

Figures 7.5 and 7.6 display the effectiveness factor versus Thiele modulus relationship given in Equation 7.29.

The raw picture

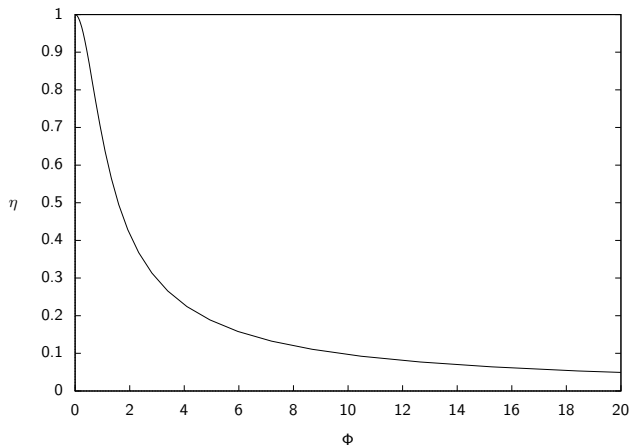


Figure 7.5: Effectiveness factor versus Thiele modulus for a first-order reaction in a sphere.

The usual plot

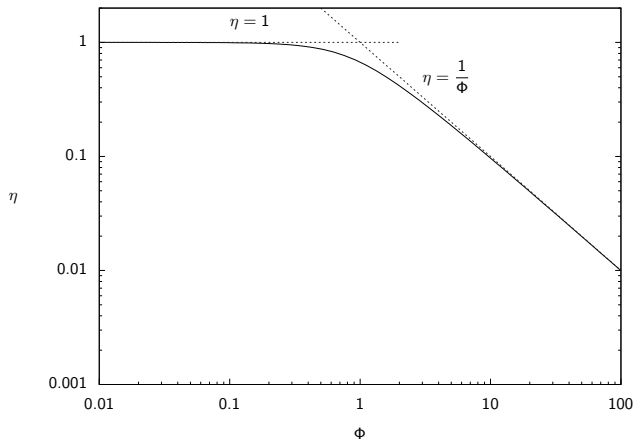


Figure 7.6: Effectiveness factor versus Thiele modulus for a first-order reaction in a sphere (log-log scale).

The log-log scale in Figure 7.6 is particularly useful, and we see the two asymptotic limits of Equation 7.29.

At small Φ , $\eta \approx 1$, and at large Φ , $\eta \approx 1/\Phi$.

Figure 7.6 shows that the asymptote $\eta = 1/\Phi$ is an excellent approximation for the spherical pellet for $\Phi \geq 10$.

For large values of the Thiele modulus, the rate of reaction is much greater than the rate of diffusion, the effectiveness factor is much less than unity, and we say the pellet is *diffusion limited*.

Conversely, when the diffusion rate is much larger than the reaction rate, the effectiveness factor is near unity, and we say the pellet is *reaction limited*.

Example 7.1: Using the Thiele modulus and effectiveness factor

The first-order, irreversible reaction ($A \rightarrow B$) takes place in a 0.3 cm radius spherical catalyst pellet at $T = 450$ K.

At 0.7 atm partial pressure of A, the pellet's production rate is -2.5×10^{-5} mol/(g s). Determine the production rate at the same temperature in a 0.15 cm radius spherical pellet.

The pellet density is $\rho_p = 0.85$ g/cm³. The effective diffusivity of A in the pellet is $D_A = 0.007$ cm²/s. □

We can use the production rate and pellet parameters for the 0.3 cm pellet to find the value for the rate constant k , and then compute the Thiele modulus, effectiveness factor and production rate for the smaller pellet.

We have three unknowns, k , Φ , η , and the following three equations

$$R_{Ap} = -\eta k c_{As} \quad (7.30)$$

$$\Phi = \sqrt{\frac{ka^2}{D_A}} \quad (7.31)$$

$$\eta = \frac{1}{\Phi} \left[\frac{1}{\tanh 3\Phi} - \frac{1}{3\Phi} \right] \quad (7.32)$$

The production rate is given in the problem statement.

Solving Equation 7.31 for k , and substituting that result and Equation 7.32 into 7.30, give one equation in the unknown Φ

$$\Phi \left[\frac{1}{\tanh 3\Phi} - \frac{1}{3\Phi} \right] = -\frac{R_{Ap}a^2}{D_A c_{As}} \quad (7.33)$$

The surface concentration and pellet production rates are given by

$$c_{As} = \frac{0.7 \text{ atm}}{\left(82.06 \frac{\text{cm}^3 \text{ atm}}{\text{mol K}}\right) (450 \text{ K})} = 1.90 \times 10^{-5} \text{ mol/cm}^3$$

$$R_{Ap} = \left(-2.5 \times 10^{-5} \frac{\text{mol}}{\text{g s}}\right) \left(0.85 \frac{\text{g}}{\text{cm}^3}\right) = -2.125 \frac{\text{mol}}{\text{cm}^3 \text{ s}}$$

Substituting these values into Equation 7.33 gives

$$\Phi \left[\frac{1}{\tanh 3\Phi} - \frac{1}{3\Phi} \right] = 1.60$$

This equation can be solved numerically yielding the Thiele modulus

$$\Phi = 1.93$$

Using this result, Equation 7.31 gives the rate constant

$$k = 2.61 \text{ s}^{-1}$$

The smaller pellet is half the radius of the larger pellet, so the Thiele modulus is half as large or $\Phi = 0.964$, which gives $\eta = 0.685$.

The production rate is therefore

$$R_{Ap} = -0.685 \left(2.6\text{s}^{-1}\right) \left(1.90 \times 10^{-5}\text{mol/cm}^3\right) = -3.38 \times 10^{-5} \frac{\text{mol}}{\text{cm}^3 \text{s}}$$

We see that decreasing the pellet size increases the production rate by almost 60%. Notice that this type of increase is possible only when the pellet is in the diffusion-limited regime.

Here we consider the cylinder and slab geometries in addition to the sphere covered in the previous section.

To have a simple analytical solution, we must neglect the end effects.

We therefore consider in addition to the sphere of radius R_s , the semi-infinite cylinder of radius R_c , and the semi-infinite slab of thickness $2L$, depicted in Figure 7.7.

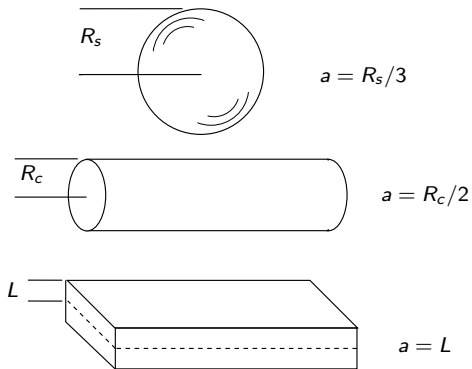


Figure 7.7: Characteristic length a for sphere, semi-infinite cylinder and semi-infinite slab.

We can summarize the reaction-diffusion mass balance for these three geometries by

$$D_A \frac{1}{r^q} \frac{d}{dr} \left(r^q \frac{dc_A}{dr} \right) - k_{cA} = 0 \quad (7.34)$$

in which

$q = 2$ sphere

$q = 1$ cylinder

$q = 0$ slab

The associated boundary conditions are

$$c_A = c_{As} \quad \left\{ \begin{array}{ll} r = R_s & \text{sphere} \\ r = R_c & \text{cylinder} \\ r = L & \text{slab} \end{array} \right.$$
$$\frac{dc_A}{dr} = 0 \quad r = 0 \quad \text{all geometries}$$

The characteristic length a is again best defined as the volume-to-surface ratio, which gives for these geometries

$$a = \frac{R_s}{3} \quad \text{sphere}$$

$$a = \frac{R_c}{2} \quad \text{cylinder}$$

$$a = L \quad \text{slab}$$

The dimensionless form of Equation 7.34 is

$$\frac{1}{\bar{r}^q} \frac{d}{d\bar{r}} \left(\bar{r}^q \frac{d\bar{c}}{d\bar{r}} \right) - \Phi^2 \bar{c} = 0 \quad (7.35)$$

$$\bar{c} = 1 \quad \bar{r} = q + 1$$

$$\frac{d\bar{c}}{d\bar{r}} = 0 \quad \bar{r} = 0$$

in which the boundary conditions for all three geometries can be compactly expressed in terms of q .

The effectiveness factor for the different geometries can be evaluated using the integral and flux approaches, Equations 7.24–7.25, which lead to the two expressions

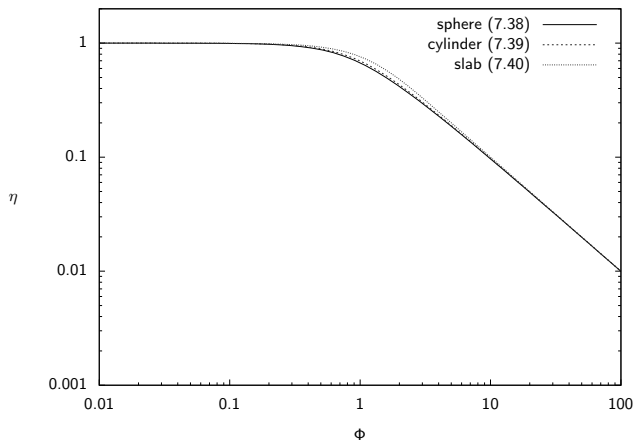
$$\eta = \frac{1}{(q+1)^q} \int_0^{q+1} \bar{c} r^q dr \quad (7.36)$$

$$\eta = \frac{1}{\Phi^2} \left. \frac{d\bar{c}}{dr} \right|_{\bar{r}=q+1} \quad (7.37)$$

We have already solved Equations 7.35 and 7.36 (or 7.37) for the sphere, $q = 2$. Analytical solutions for the slab and cylinder geometries also can be derived. See Exercise 7.1 for the slab geometry. The results are summarized in the following table.

Sphere	$\eta = \frac{1}{\Phi} \left[\frac{1}{\tanh 3\Phi} - \frac{1}{3\Phi} \right] \quad (7.38)$
Cylinder	$\eta = \frac{1}{\Phi} \frac{I_1(2\Phi)}{I_0(2\Phi)} \quad (7.39)$
Slab	$\eta = \frac{\tanh \Phi}{\Phi} \quad (7.40)$

The effectiveness factors versus Thiele modulus for the three geometries are



Use the right Φ and ignore geometry!

Although the functional forms listed in the table appear quite different, we see in the figure that these solutions are quite similar.

The effectiveness factor for the slab is largest, the cylinder is intermediate, and the sphere is the smallest at all values of Thiele modulus.

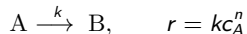
The three curves have identical small Φ and large Φ asymptotes.

The maximum difference between the effectiveness factors of the sphere and the slab η is about 16%, and occurs at $\Phi = 1.6$. For $\Phi < 0.5$ and $\Phi > 7$, the difference between all three effectiveness factors is less than 5%.

For reactions other than first order, the reaction-diffusion equation is nonlinear and numerical solution is required.

We will see, however, that many of the conclusions from the analysis of the first-order reaction case still apply for other reaction orders.

We consider n th-order, irreversible reaction kinetics



The reaction-diffusion equation for this case is

$$D_A \frac{1}{r^q} \frac{d}{dr} \left(r^q \frac{dc_A}{dr} \right) - kc_A^n = 0 \quad (7.41)$$

The results for various reaction orders have a common asymptote if we instead define

$$\Phi = \sqrt{\frac{n+1}{2} \frac{kc_{As}^{n-1} a^2}{D_A}} \quad \begin{array}{l} \text{Thiele modulus} \\ \text{nth-order reaction} \end{array} \quad (7.42)$$

$$\frac{1}{\bar{r}^q} \frac{d}{d\bar{r}} \left(\bar{r}^q \frac{d\bar{c}}{d\bar{r}} \right) - \frac{2}{n+1} \Phi^2 \bar{c}^n = 0$$

$$\bar{c} = 1 \quad \bar{r} = q + 1$$

$$\frac{d\bar{c}}{d\bar{r}} = 0 \quad \bar{r} = 0$$

$$\eta = \frac{1}{(q+1)^q} \int_0^{q+1} \bar{c}^n \bar{r}^q d\bar{r}$$

$$\eta = \frac{n+1}{2} \frac{1}{\Phi^2} \left. \frac{d\bar{c}}{d\bar{r}} \right|_{\bar{r}=q+1}$$

Figure 7.9 shows the effect of reaction order for $n \geq 1$ in a spherical pellet. As the reaction order increases, the effectiveness factor decreases. Notice that the definition of Thiele modulus in Equation 7.42 has achieved the desired goal of giving all reaction orders a common asymptote at high values of Φ .

Reaction order greater than one

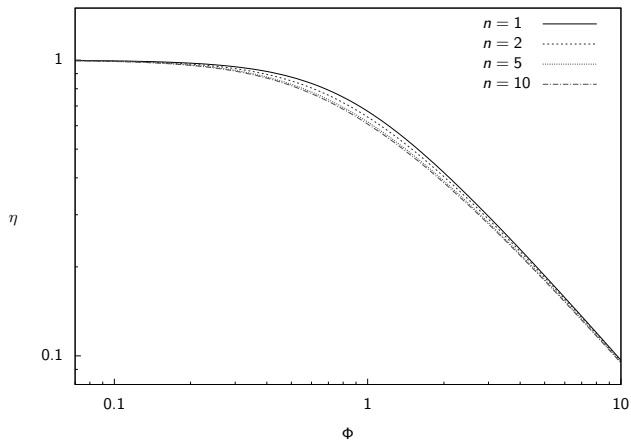


Figure 7.9: Effectiveness factor versus Thiele modulus in a spherical pellet; reaction orders greater than unity.

Figure 7.10 shows the effectiveness factor versus Thiele modulus for reaction orders less than unity.

Notice the discontinuity in slope of the effectiveness factor versus Thiele modulus that occurs when the order is less than unity.

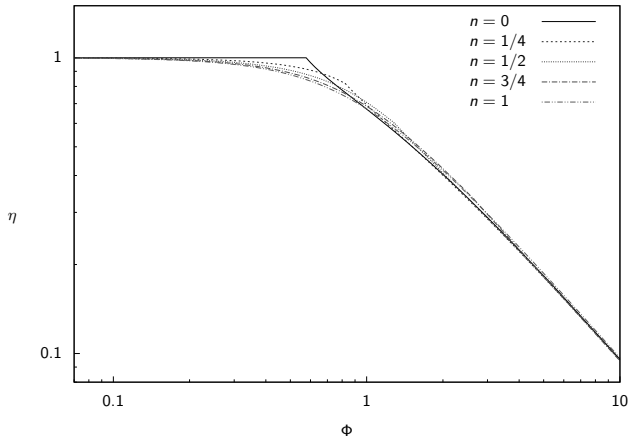


Figure 7.10: Effectiveness factor versus Thiele modulus in a spherical pellet; reaction orders less than unity.

Recall from the discussion in Chapter 4 that if the reaction order is less than unity in a batch reactor, the concentration of A reaches zero in finite time.

In the reaction-diffusion problem in the pellet, the same kinetic effect causes the discontinuity in η versus Φ .

For large values of Thiele modulus, the diffusion is slow compared to reaction, and the A concentration reaches zero at some nonzero radius inside the pellet.

For orders less than unity, an inner region of the pellet has identically zero A concentration.

Figure 7.11 shows the reactant concentration versus radius for the zero-order reaction case in a sphere at various values of Thiele modulus.

Reaction order less than one II

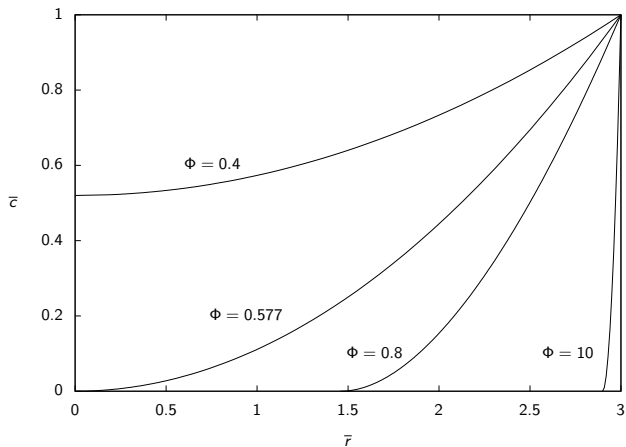


Figure 7.11: Dimensionless concentration versus radius for zero-order reaction ($n = 0$) in a spherical pellet ($q = 2$); for large Φ the inner region of the pellet has zero A concentration.

Use the right Φ and ignore reaction order!

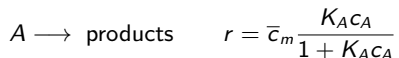
Using the Thiele modulus

$$\Phi = \sqrt{\frac{n+1}{2} \frac{kC_{As}^{n-1} a^2}{D_A}}$$

allows us to approximate all orders with the analytical result derived for first order.
The approximation is fairly accurate and we don't have to solve the problem numerically.

Given the discussion in Section 5.6 of adsorption and reactions on catalyst surfaces, it is reasonable to expect our best catalyst rate expressions may be of the Hougen-Watson form.

Consider the following reaction and rate expression



This expression arises when gas-phase A adsorbs onto the catalyst surface and the reaction is first order in the adsorbed A concentration.

If we consider the slab catalyst geometry, the mass balance is

$$D_A \frac{d^2 c_A}{dr^2} - k \bar{c}_m \frac{K_{A C_A}}{1 + K_{A C_A}} = 0$$

and the boundary conditions are

$$\begin{aligned} c_A &= c_{A_s} & r &= L \\ \frac{dc_A}{dr} &= 0 & r &= 0 \end{aligned}$$

We would like to study the effectiveness factor for these kinetics.

First we define dimensionless concentration and length as before to arrive at the dimensionless reaction-diffusion model

$$\frac{d^2\bar{c}}{d\bar{r}^2} - \tilde{\Phi}^2 \frac{\bar{c}}{1 + \phi\bar{c}} = 0 \quad (7.43)$$

$$\begin{aligned} \bar{c} = 1 & \quad \bar{r} = 1 \\ \frac{d\bar{c}}{d\bar{r}} = 0 & \quad \bar{r} = 0 \end{aligned} \quad (7.44)$$

in which we now have *two* dimensionless groups

$$\tilde{\Phi} = \sqrt{\frac{k\bar{c}_m K_A a^2}{D_A}}, \quad \phi = K_A c_{A_s} \quad (7.45)$$

We use the tilde to indicate $\tilde{\Phi}$ is a good first guess for a Thiele modulus for this problem, but we will find a better candidate subsequently.

The new dimensionless group ϕ represents a dimensionless adsorption constant.

The effectiveness factor is calculated from

$$\eta = \frac{R_{Ap}}{R_{As}} = \frac{-(S_p/V_p)D_A dc_A/dr|_{r=a}}{-k\bar{c}_m K_{ACAs}/(1 + K_{ACAs})}$$

which becomes upon definition of the dimensionless quantities

$$\eta = \frac{1 + \phi}{\tilde{\Phi}^2} \left. \frac{d\bar{c}}{d\bar{r}} \right|_{\bar{r}=1} \quad (7.46)$$

Now we wish to define a Thiele modulus so that η has a common asymptote at large Φ for all values of ϕ .

This goal was accomplished for the n th-order reaction as shown in Figures 7.9 and 7.10 by including the factor $(n + 1)/2$ in the definition of Φ given in Equation 7.42.

The text shows how to do this analysis, which was developed independently by *four* chemical engineers.

What did ChE professors work on in the 1960s?

This idea appears to have been discovered independently by *three* chemical engineers in 1965.

To quote from Aris [2, p. 113]

This is the essential idea in three papers published independently in March, May and June of 1965; see Bischoff [4], Aris [1] and Petersen [10]. A more limited form was given as early as 1958 by Stewart in Bird, Stewart and Lightfoot [3, p. 338].

The rescaling is accomplished by

$$\Phi = \left(\frac{\phi}{1 + \phi} \right) \frac{1}{\sqrt{2(\phi - \ln(1 + \phi))}} \tilde{\Phi}$$

So we have the following two dimensionless groups for this problem

$$\Phi = \left(\frac{\phi}{1 + \phi} \right) \sqrt{\frac{k\bar{c}_m K_A a^2}{2D_A(\phi - \ln(1 + \phi))}}, \quad \phi = K_A c_{A_s} \quad (7.52)$$

The payoff for this analysis is shown in Figures 7.13 and 7.14.

The first attempt

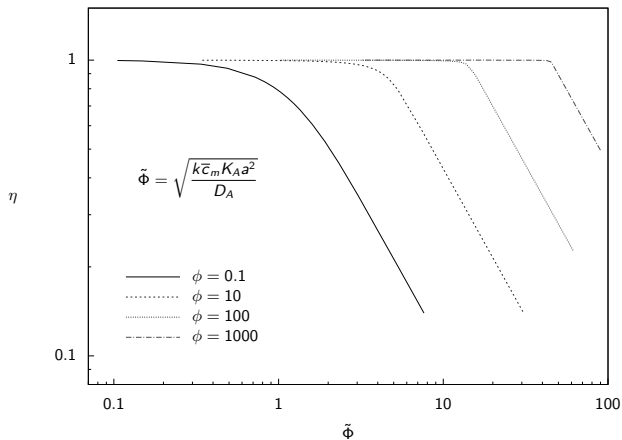


Figure 7.13: Effectiveness factor versus an inappropriate Thiele modulus in a slab; Hugen-Watson kinetics.

The right rescaling

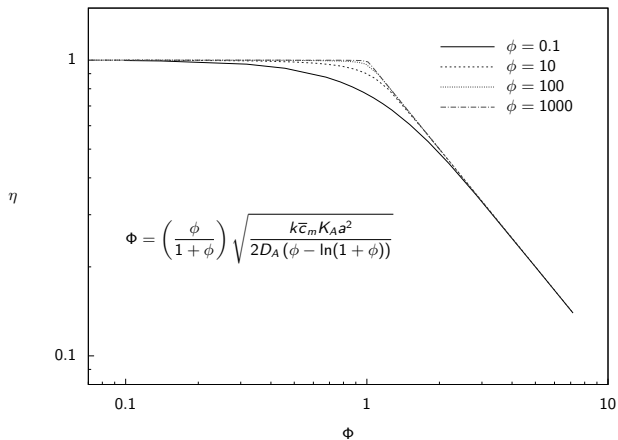


Figure 7.14: Effectiveness factor versus appropriate Thiele modulus in a slab; Høugen-Watson kinetics.

Use the right Φ and ignore the reaction form!

If we use our first guess for the Thiele modulus, Equation 7.45, we obtain Figure 7.13 in which the various values of ϕ have different asymptotes.

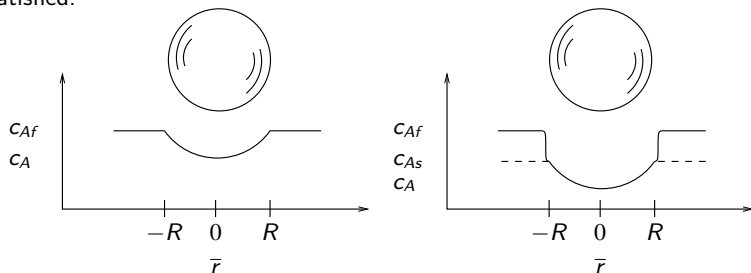
Using the Thiele modulus defined in Equation 7.52, we obtain the results in Figure 7.14. Figure 7.14 displays things more clearly.

Again we see that as long as we choose an appropriate Thiele modulus, we can approximate the effectiveness factor for all values of ϕ with the first-order reaction. The largest approximation error occurs near $\Phi = 1$, and if $\Phi > 2$ or $\Phi < 0.2$, the approximation error is negligible.

If the mass-transfer rate from the bulk fluid to the exterior of the pellet is not high, then the boundary condition

$$c_A(r = R) = c_{Af}$$

is not satisfied.



To obtain a simple model of the external mass transfer, we replace the boundary condition above with a flux boundary condition

$$D_A \frac{dc_A}{dr} = k_m (c_{Af} - c_A), \quad r = R \quad (7.53)$$

in which k_m is the external mass-transfer coefficient.

If we multiply Equation 7.53 by $a/c_{Af}D_A$, we obtain the dimensionless boundary condition

$$\frac{d\bar{c}}{d\bar{r}} = B(1 - \bar{c}), \quad \bar{r} = 3 \quad (7.54)$$

in which

$$B = \frac{k_m a}{D_A} \quad (7.55)$$

is the Biot number or dimensionless mass-transfer coefficient.

Summarizing, for finite external mass transfer, the dimensionless model and boundary conditions are

$$\frac{1}{\bar{r}^2} \frac{d}{d\bar{r}} \left(\bar{r}^2 \frac{d\bar{c}}{d\bar{r}} \right) - \Phi^2 \bar{c} = 0 \quad (7.56)$$

$$\frac{d\bar{c}}{d\bar{r}} = B(1 - \bar{c}) \quad \bar{r} = 3$$

$$\frac{d\bar{c}}{d\bar{r}} = 0 \quad \bar{r} = 0$$

The solution to the differential equation satisfying the center boundary condition can be derived as in Section 7.4 to produce

$$\bar{c}(\bar{r}) = \frac{c_2}{\bar{r}} \sinh \Phi \bar{r}$$

in which c_2 is the remaining unknown constant. Evaluating this constant using the external boundary condition gives

$$\bar{c}(\bar{r}) = \frac{3}{\bar{r}} \frac{\sinh \Phi \bar{r}}{\sinh 3\Phi + (\Phi \cosh 3\Phi - (\sinh 3\Phi)/3)/B} \quad (7.57)$$

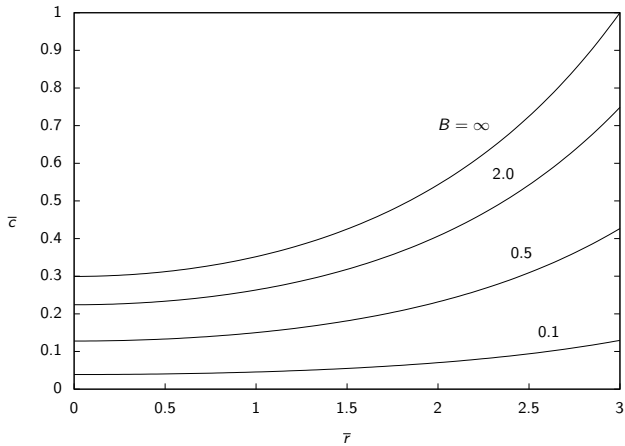


Figure 7.16: Dimensionless concentration versus radius for different values of the Biot number; first-order reaction in a spherical pellet with $\Phi = 1$.

The effectiveness factor can again be derived by integrating the local reaction rate or computing the surface flux, and the result is

$$\eta = \frac{1}{\Phi} \left[\frac{1/\tanh 3\Phi - 1/(3\Phi)}{1 + \Phi (1/\tanh 3\Phi - 1/(3\Phi))/B} \right] \quad (7.58)$$

in which

$$\eta = \frac{R_{Ap}}{R_{Ab}}$$

Notice we are comparing the pellet's reaction rate to the rate that would be achieved if the pellet reacted at the *bulk fluid concentration* rather than the pellet exterior concentration as before.

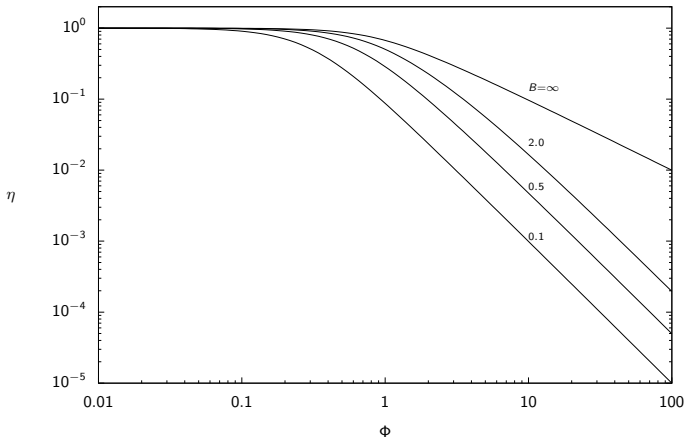


Figure 7.17: Effectiveness factor versus Thiele modulus for different values of the Biot number; first-order reaction in a spherical pellet.

Figure 7.17 shows the effect of the Biot number on the effectiveness factor or total pellet reaction rate.

Notice that the slope of the log-log plot of η versus Φ has a slope of negative *two* rather than negative one as in the case without external mass-transfer limitations ($B = \infty$).

Figure 7.18 shows this effect in more detail.

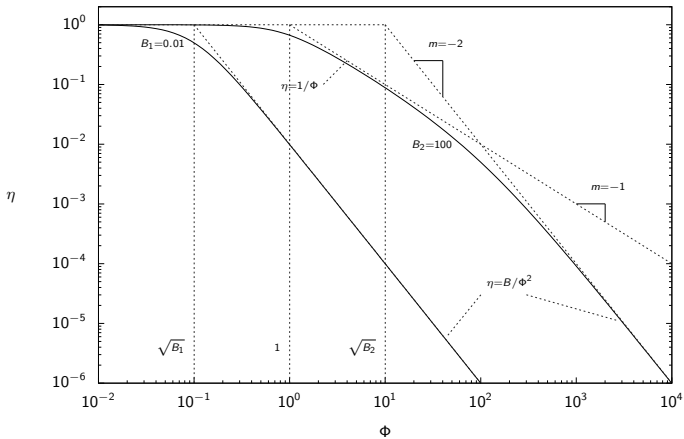


Figure 7.18: Asymptotic behavior of the effectiveness factor versus Thiele modulus; first-order reaction in a spherical pellet.

If B is small, the log-log plot corners with a slope of negative two at $\Phi = \sqrt{B}$.

If B is large, the log-log plot first corners with a slope of negative one at $\Phi = 1$, then it corners again and decreases the slope to negative two at $\Phi = \sqrt{B}$.

Both mechanisms of diffusional resistance, the diffusion within the pellet and the mass transfer from the fluid to the pellet, show their effect on pellet reaction rate by changing the slope of the effectiveness factor by negative one.

Given the value of the Biot number, one can easily sketch the straight line asymptotes shown in Figure 7.18. Then, given the value of the Thiele modulus, one can determine the approximate concentration profile, and whether internal diffusion or external mass transfer or both limit the pellet reaction rate.

Which mechanism controls?

The possible cases are summarized in the table

Biot number	Thiele modulus	Mechanism controlling pellet reaction rate
$B < 1$	$\Phi < B$ $B < \Phi < 1$ $1 < \Phi$	reaction external mass transfer both external mass transfer and internal diffusion
$1 < B$	$\Phi < 1$ $1 < \Phi < B$ $B < \Phi$	reaction internal diffusion both internal diffusion and external mass transfer

Table 7.4: The controlling mechanisms for pellet reaction rate given finite rates of internal diffusion and external mass transfer.

- We often need to determine a reaction order and rate constant for some catalytic reaction of interest.
- Assume the following n th-order reaction takes place in a catalyst particle



- We call the values of k and n the intrinsic rate constant and reaction order to distinguish them from what we may estimate from data.
- The typical experiment is to change the value of c_A in the bulk fluid, measure the rate r_1 as a function of c_A , and then find the values of the parameters k and n that best fit the measurements.

Here we show only that one should exercise caution with this estimation if we are measuring the rates with a solid catalyst. The effects of reaction, diffusion and external mass transfer may all manifest themselves in the measured rate.

We express the reaction rate as

$$r_1 = \eta k c_{Ab}^n \quad (7.59)$$

We also know that at steady state, the rate is equal to the flux of A into the catalyst particle

$$r_1 = k_{mA}(c_{Ab} - c_{As}) = \frac{D_A}{a} \left. \frac{dc_A}{dr} \right|_{r=R} \quad (7.60)$$

We now study what happens to our experiment under different rate-limiting steps.

First assume that both the external mass transfer and internal pellet diffusion are fast compared to the reaction. Then $\eta = 1$, and we would estimate the intrinsic parameters correctly in Equation 7.59

$$k_{ob} = k$$

$$n_{ob} = n$$

Everything goes according to plan when we are reaction limited.

Next assume that the external mass transfer and reaction are fast, but the internal diffusion is slow. In this case we have $\eta = 1/\Phi$, and using the definition of Thiele modulus and Equation 7.59

$$r_1 = k_{\text{ob}} c_{A_s}^{(n+1)/2} \quad (7.61)$$

$$k_{\text{ob}} = \frac{1}{a} \sqrt{\frac{2}{n+1}} D_A \sqrt{k} \quad (7.62)$$

$$n_{\text{ob}} = (n+1)/2 \quad (7.63)$$

So we see two problems. The rate constant we estimate, k_{ob} , varies as the square root of the intrinsic rate constant, k . The diffusion has affected the measured rate of the reaction and disguised the rate constant.

We even get an incorrect reaction order: a first-order reaction appears half-order, a second-order reaction appears first-order, and so on.

$$r_1 = k_{\text{ob}} c_{A_s}^{(n+1)/2}$$
$$k_{\text{ob}} = \frac{1}{a} \sqrt{\frac{2}{n+1}} D_A \sqrt{k}$$
$$n_{\text{ob}} = (n+1)/2$$

Also consider what happens if we vary the temperature and try to determine the reaction's activation energy.

Let the temperature dependence of the diffusivity, D_A , be represented also in Arrhenius form, with E_{diff} the activation energy of the diffusion coefficient.

Let E_{rxn} be the intrinsic activation energy of the reaction. The observed activation energy from Equation 7.62 is

$$E_{\text{ob}} = \frac{E_{\text{diff}} + E_{\text{rxn}}}{2}$$

so both activation energies show up in our estimated activation energy.

Normally the temperature dependence of the diffusivity is much smaller than the temperature dependence of the reaction, $E_{\text{diff}} \ll E_{\text{rxn}}$, so we would estimate an activation energy that is one-half the intrinsic value.

Finally, assume the reaction and diffusion are fast compared to the external mass transfer. Then we have $c_{Ab} \gg c_{As}$ and Equation 7.60 gives

$$r_1 = k_{mA}c_{Ab}$$

If we vary c_{Ab} and measure r_1 , we would find the mass transfer coefficient instead of the rate constant, and a first-order reaction instead of the true reaction order

$$k_{\text{ob}} = k_{mA}$$

$$n_{\text{ob}} = 1$$

Normally, mass-transfer coefficients also have fairly small temperature dependence compared to reaction rates, so the observed activation energy would be almost zero, independent of the true reaction's activation energy.

Mass transfer and diffusion resistances *disguise* the reaction kinetics.

We can solve this problem in two ways. First, we can arrange the experiment so that mass transfer and diffusion are fast and do not affect the estimates of the kinetic parameters. How?

If this approach is impractical or too expensive, we can alternatively model the effects of the mass transfer and diffusion, and estimate the parameters D_A and k_{mA} simultaneously with k and n . We develop techniques in Chapter 9 to handle this more complex estimation problem.

- We now consider situations in which the catalyst particle is not isothermal.
- Given an exothermic reaction, for example, if the particle's thermal conductivity is not large compared to the rate of heat release due to chemical reaction, the temperature rises inside the particle.
- We wish to explore the effects of this temperature rise on the catalyst performance.

- We have already written the general mass and energy balances for the catalyst particle in Section 7.3.

$$0 = D_j \nabla^2 c_j + R_j, \quad j = 1, 2, \dots, n_s$$

$$0 = \hat{k} \nabla^2 T - \sum_i \Delta H_{Ri} r_i$$

- Consider the single-reaction case, in which we have $R_A = -r$ and Equations 7.14 and 7.15 reduce to

$$D_A \nabla^2 c_A = r$$

$$\hat{k} \nabla^2 T = \Delta H_R r$$

- We can eliminate the reaction term between the mass and energy balances to produce

$$\nabla^2 T = \frac{\Delta H_R D_A}{\hat{k}} \nabla^2 c_A$$

which relates the conversion of the reactant to the rise (or fall) in temperature.

- Because we have assumed constant properties, we can integrate this equation twice to give the relationship between temperature and A concentration

$$T - T_s = \frac{-\Delta H_R D_A}{\hat{k}} (c_{As} - c_A) \quad (7.64)$$

We now consider a first-order reaction and assume the rate constant has an Arrhenius form,

$$k(T) = k_s \exp \left[-E \left(\frac{1}{T} - \frac{1}{T_s} \right) \right]$$

in which T_s is the pellet exterior temperature, and we assume fast external mass transfer. Substituting Equation 7.64 into the rate constant expression gives

$$k(T) = k_s \exp \left[\frac{E}{T_s} \left(1 - \frac{T_s}{T_s + \Delta H_R D_A (c_A - c_{As}) / \hat{k}} \right) \right]$$

We can simplify matters by defining three dimensionless variables

$$\gamma = \frac{E}{T_s}, \quad \beta = \frac{-\Delta H_R D_A c_{As}}{\hat{k} T_s}, \quad \tilde{\Phi}^2 = \frac{k(T_s)}{D_A} a^2$$

in which γ is a dimensionless activation energy, β is a dimensionless heat of reaction, and $\tilde{\Phi}$ is the usual Thiele modulus. Again we use the tilde to indicate we will find a better Thiele modulus subsequently.

With these variables, we can express the rate constant as

$$k(T) = k_s \exp \left[\frac{\gamma \beta (1 - \bar{c})}{1 + \beta (1 - \bar{c})} \right]$$

We then substitute the rate constant into the mass balance, and assume a spherical particle to obtain the final dimensionless model

$$\begin{aligned} \frac{1}{\bar{r}^2} \frac{d}{d\bar{r}} \left(\bar{r}^2 \frac{d\bar{c}}{d\bar{r}} \right) &= \tilde{\Phi}^2 \bar{c} \exp \left(\frac{\gamma\beta(1-\bar{c})}{1+\beta(1-\bar{c})} \right) \\ \frac{d\bar{c}}{d\bar{r}} &= 0 \quad \bar{r} = 3 \\ \bar{c} &= 1 \quad \bar{r} = 0 \end{aligned} \tag{7.65}$$

Equation 7.65 is sometimes called the Weisz-Hicks problem in honor of Weisz and Hicks's outstanding paper in which they computed accurate numerical solutions to this problem [13].

Given the solution to Equation 7.65, we can compute the effectiveness factor for the nonisothermal pellet using the usual relationship

$$\eta = \frac{1}{\tilde{\Phi}^2} \left. \frac{d\bar{c}}{d\bar{r}} \right|_{\bar{r}=3}$$

If we perform the same asymptotic analysis of Section 7.4.4 on the Weisz-Hicks problem, we find, however, that the appropriate Thiele modulus for this problem is

$$\Phi = \tilde{\Phi}/I(\gamma, \beta), \quad I(\gamma, \beta) = \left[2 \int_0^1 c \exp\left(\frac{\gamma\beta(1-c)}{1+\beta(1-c)}\right) dc \right]^{1/2} \quad (7.66)$$

The normalizing integral $I(\gamma, \beta)$ can be expressed as a sum of exponential integrals [2] or evaluated by quadrature.

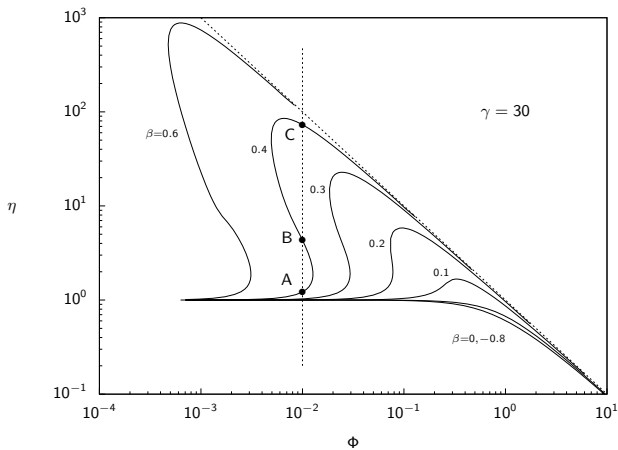
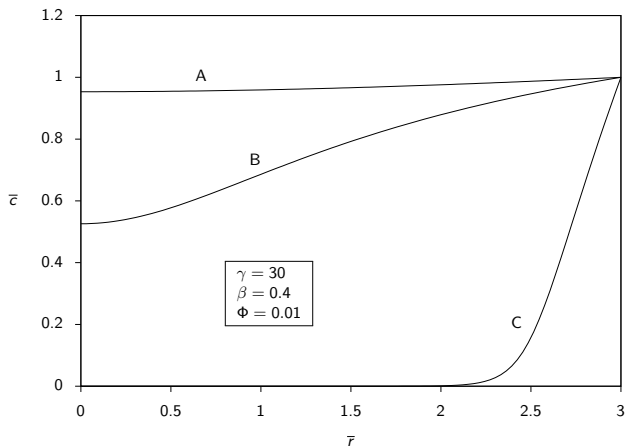


Figure 7.19: Effectiveness factor versus normalized Thiele modulus for a first-order reaction in a nonisothermal spherical pellet.

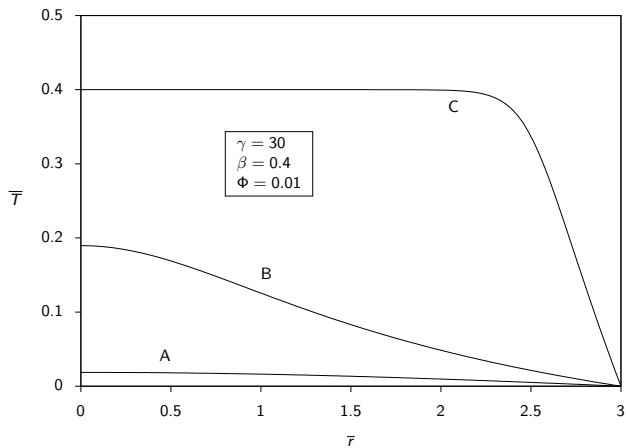
- Note that Φ is well chosen in Equation 7.66 because the large Φ asymptotes are the same for all values of γ and β .
- The first interesting feature of Figure 7.19 is that the effectiveness factor is *greater than unity* for some values of the parameters.
- Notice that feature is more pronounced as we increase the exothermic heat of reaction.
- For the highly exothermic case, the pellet's interior temperature is significantly *higher* than the exterior temperature T_s . The rate constant inside the pellet is therefore much larger than the value at the exterior, k_s . This leads to η greater than unity.

- A second striking feature of the nonisothermal pellet is that multiple steady states are possible.
- Consider the case $\Phi = 0.01$, $\beta = 0.4$ and $\gamma = 30$ shown in Figure 7.19.
- The effectiveness factor has three possible values for this case.
- We show in the next two figures the solution to Equation 7.65 for this case.

The concentration profile



And the temperature profile



- The three temperature and concentration profiles correspond to an ignited steady state (C), an extinguished steady state (A), and an unstable intermediate steady state (B).
- As we showed in Chapter 6, whether we achieve the ignited or extinguished steady state in the pellet depends on how the reactor is started.
- For realistic values of the catalyst thermal conductivity, however, the pellet can often be considered isothermal and the energy balance can be neglected [9].
- *Multiple steady-state solutions in the particle may still occur in practice, however, if there is a large external heat transfer resistance.*

- As the next step up in complexity, we consider the case of multiple reactions.
- Even numerical solution of some of these problems is challenging for two reasons.
- First, steep concentration profiles often occur for realistic parameter values, and we wish to compute these profiles accurately. It is not unusual for species concentrations to change by 10 orders of magnitude within the pellet for realistic reaction and diffusion rates.
- Second, we are solving boundary-value problems because the boundary conditions are provided at the center and exterior surface of the pellet.
- We use the collocation method, which is described in more detail in Appendix A.

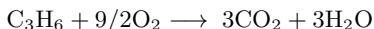
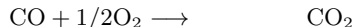
Multiple reaction example—Catalytic converter

The next example involves five species, two reactions with Hougen-Watson kinetics, and both diffusion and external mass-transfer limitations.

Example 7.2: Catalytic converter

Consider the oxidation of CO and a representative volatile organic such as propylene in a automobile catalytic converter containing spherical catalyst pellets with particle radius 0.175 cm.

The particle is surrounded by a fluid at 1.0 atm pressure and 550 K containing 2% CO, 3% O₂ and 0.05% (500 ppm) C₃H₆. The reactions of interest are



with rate expressions given by Oh et al. [8]

$$r_1 = \frac{k_1 c_{\text{CO}} c_{\text{O}_2}}{(1 + K_{\text{CO}} c_{\text{CO}} + K_{\text{C}_3\text{H}_6} c_{\text{C}_3\text{H}_6})^2}$$

$$r_2 = \frac{k_2 c_{\text{C}_3\text{H}_6} c_{\text{O}_2}}{(1 + K_{\text{CO}} c_{\text{CO}} + K_{\text{C}_3\text{H}_6} c_{\text{C}_3\text{H}_6})^2}$$

The rate constants and the adsorption constants are assumed to have Arrhenius form. The parameter values are given in Table 7.5 [8].
The pellet may be assumed to be isothermal.
Calculate the steady-state pellet concentration profiles of all reactants and products.

Parameter	Value	Units	Parameter	Value	Units
P	1.013×10^5	N/m ²	k_{10}	7.07×10^{19}	cm ³ /mol·s
T	550	K	k_{20}	1.47×10^{21}	cm ³ /mol·s
R	0.175	cm	K_{COO}	8.099×10^6	cm ³ /mol
E_1	13,108	K	$K_{C_3H_6O}$	2.579×10^8	cm ³ /mol
E_2	15,109	K	D_{CO}	0.0487	cm ² /s
E_{CO}	-409	K	D_{O_2}	0.0469	cm ² /s
$E_{C_3H_6}$	191	K	$D_{C_3H_6}$	0.0487	cm ² /s
$c_{CO}f$	2.0 %		k_{mCO}	3.90	cm/s
$c_{O_2}f$	3.0 %		k_{mO_2}	4.07	cm/s
$c_{C_3H_6}f$	0.05 %		$k_{mC_3H_6}$	3.90	cm/s

Table 7.5: Kinetic and mass-transfer parameters for the catalytic converter example.

We solve the steady-state mass balances for the three reactant species,

$$D_j \frac{1}{r^2} \frac{d}{dr} \left(r^2 \frac{dc_j}{dr} \right) = -R_j$$

with the boundary conditions

$$\begin{aligned} \frac{dc_j}{dr} &= 0 & r &= 0 \\ D_j \frac{dc_j}{dr} &= k_{mj} (c_{jf} - c_j) & r &= R \end{aligned}$$

$j = \{\text{CO}, \text{O}_2, \text{C}_3\text{H}_6\}$. The model is solved using the collocation method. The reactant concentration profiles are shown in Figures 7.22 and 7.23.

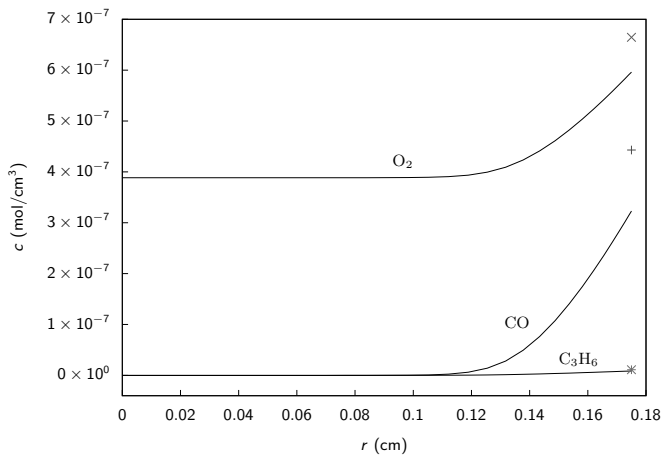


Figure 7.22: Concentration profiles of reactants; fluid concentration of O_2 (\times), CO ($+$), C_3H_6 ($*$).

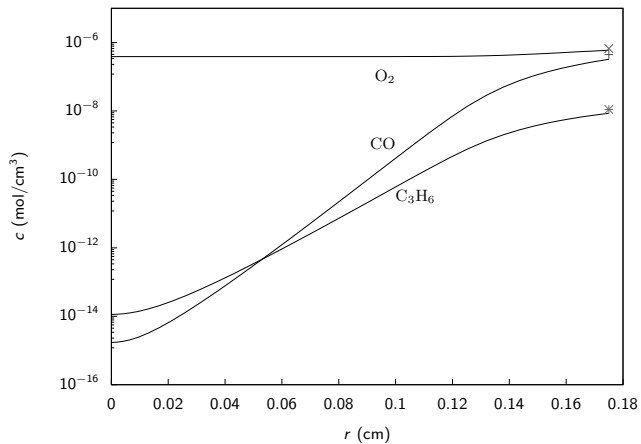


Figure 7.23: Concentration profiles of reactants (log scale); fluid concentration of O_2 (\times), CO ($+$), C_3H_6 ($*$).

Notice that O_2 is in excess and both CO and C_3H_6 reach very low values within the pellet.

The log scale in Figure 7.23 shows that the concentrations of these reactants change by seven orders of magnitude.

Obviously the consumption rate is large compared to the diffusion rate for these species. The external mass-transfer effect is noticeable, but not dramatic.

The product concentrations could simply be calculated by solving their mass balances along with those of the reactants.

Because we have only two reactions, however, the products concentrations are also computable from the stoichiometry and the mass balances.

The text shows this step in detail.

The results of the calculation are shown in the next figure.

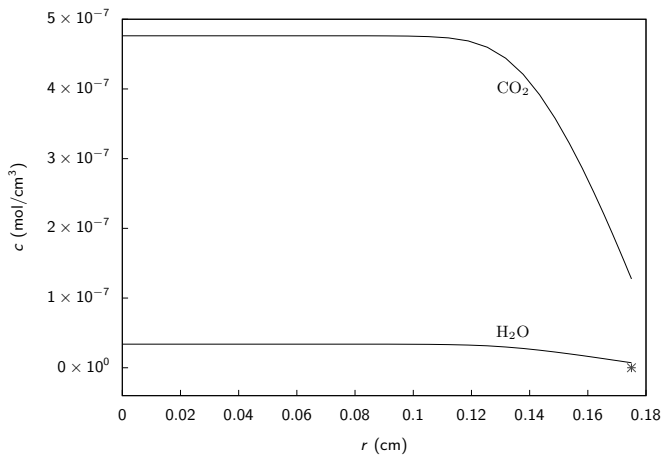


Figure 7.24: Concentration profiles of the products; fluid concentration of CO₂ (×), H₂O (+).

Notice from Figure 7.24 that CO_2 is the main product.

Notice also that the products flow out of the pellet, unlike the reactants, which are flowing into the pellet.

- Given our detailed understanding of the behavior of a single catalyst particle, we now are prepared to pack a tube with a bed of these particles and solve the fixed-bed reactor design problem.
- In the fixed-bed reactor, we keep track of two phases. The fluid-phase streams through the bed and transports the reactants and products through the reactor.
- The reaction-diffusion processes take place in the solid-phase catalyst particles.
- The two phases communicate to each other by exchanging mass and energy at the catalyst particle exterior surfaces.
- We have constructed a detailed understanding of all these events, and now we assemble them together.

We make the following assumptions:

- ① Uniform catalyst pellet exterior. Particles are small compared to the length of the reactor.
- ② Plug flow in the bed, no radial profiles.
- ③ Neglect axial diffusion in the bed.
- ④ Steady state.

In the fluid phase, we track the molar flows of all species, the temperature and the pressure.

We can no longer neglect the pressure drop in the tube because of the catalyst bed. We use an empirical correlation to describe the pressure drop in a packed tube, the well-known Ergun equation [6].

$$\begin{aligned} \frac{dN_j}{dV} &= R_j & (7.67) \\ Q\rho\hat{C}_p\frac{dT}{dV} &= -\sum_i \Delta H_{Ri}r_i + \frac{2}{R}U^o(T_a - T) \\ \frac{dP}{dV} &= -\frac{(1-\epsilon_B)}{D_p\epsilon_B^3}\frac{Q}{A_c^2}\left[150\frac{(1-\epsilon_B)\mu_f}{D_p} + \frac{7}{4}\frac{\rho Q}{A_c}\right] \end{aligned}$$

The fluid-phase boundary conditions are provided by the known feed conditions at the tube entrance

$$\begin{aligned} N_j &= N_{jf}, & z &= 0 \\ T &= T_f, & z &= 0 \\ P &= P_f, & z &= 0 \end{aligned}$$

Inside the catalyst particle, we track the concentrations of all species and the temperature.

$$D_j \frac{1}{r^2} \frac{d}{dr} \left(r^2 \frac{d\tilde{c}_j}{dr} \right) = -\tilde{R}_j$$
$$\hat{k} \frac{1}{r^2} \frac{d}{dr} \left(r^2 \frac{d\tilde{T}}{dr} \right) = \sum_i \Delta H_{Ri} \tilde{r}_i$$

The boundary conditions are provided by the mass-transfer and heat-transfer rates at the pellet exterior surface, and the zero slope conditions at the pellet center

$$\frac{d\tilde{c}_j}{dr} = 0 \quad r = 0$$
$$D_j \frac{d\tilde{c}_j}{dr} = k_{mj}(c_j - \tilde{c}_j) \quad r = R$$
$$\frac{d\tilde{T}}{dr} = 0 \quad r = 0$$
$$\hat{k} \frac{d\tilde{T}}{dr} = k_T(T - \tilde{T}) \quad r = R$$

Finally, we equate the production rate R_j experienced by the fluid phase to the production rate inside the particles, which is where the reaction takes place.

Analogously, we equate the enthalpy change on reaction experienced by the fluid phase to the enthalpy change on reaction taking place inside the particles.

$$\underbrace{R_j}_{\text{rate } j \text{ / vol}} = - \underbrace{(1 - \epsilon_B)}_{\text{vol cat / vol}} \underbrace{\frac{S_p}{V_p} D_j \frac{d\tilde{c}_j}{dr}}_{\text{rate } j \text{ / vol cat}} \Big|_{r=R}$$

$$\underbrace{\sum_i \Delta H_{Ri} r_i}_{\text{rate heat / vol}} = \underbrace{(1 - \epsilon_B)}_{\text{vol cat / vol}} \underbrace{\frac{S_p}{V_p} \hat{k} \frac{d\tilde{T}}{dr}}_{\text{rate heat / vol cat}} \Big|_{r=R} \tag{7.77}$$

We require the bed porosity (Not particle porosity!) to convert from the rate per volume of particle to the rate per volume of reactor.

The bed porosity or void fraction, ϵ_B , is defined as the volume of voids per volume of reactor.

The volume of catalyst per volume of reactor is therefore $1 - \epsilon_B$.

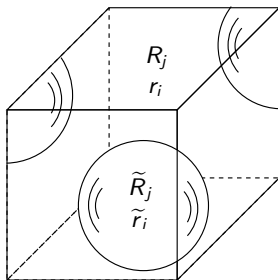
This information can be presented in a number of equivalent ways. We can easily measure the density of the pellet, ρ_p , and the density of the bed, ρ_B .

From the definition of bed porosity, we have the relation

$$\rho_B = (1 - \epsilon_B)\rho_p$$

or if we solve for the volume fraction of catalyst

$$1 - \epsilon_B = \rho_B / \rho_p$$

**Mass**

$$R_j = (1 - \epsilon_B) \tilde{R}_{jp}$$

$$\tilde{R}_{jp} = -\frac{S_p}{V_p} D_j \left. \frac{d\tilde{c}_j}{dr} \right|_{r=R}$$

Energy

$$\sum_i \Delta H_{Ri} r_i = (1 - \epsilon_B) \sum_i \Delta H_{Ri} \tilde{r}_{ip}$$

$$\sum_i \Delta H_{Ri} \tilde{r}_{ip} = \frac{S_p}{V_p} \hat{k} \left. \frac{d\tilde{T}}{dr} \right|_{r=R}$$

Figure 7.25: Fixed-bed reactor volume element containing fluid and catalyst particles; the equations show the coupling between the catalyst particle balances and the overall reactor balances.

Equations 7.67–7.77 provide the full packed-bed reactor model given our assumptions. We next examine several packed-bed reactor problems that can be solved without solving this full set of equations.

Finally, we present an example that requires numerical solution of the full set of equations.

Example 7.3: First-order, isothermal fixed-bed reactor

Use the rate data presented in Example 7.1 to find the fixed-bed reactor volume and the catalyst mass needed to convert 97% of A. The feed to the reactor is pure A at 1.5 atm at a rate of 12 mol/s. The 0.3 cm pellets are to be used, which leads to a bed density $\rho_B = 0.6 \text{ g/cm}^3$. Assume the reactor operates isothermally at 450 K and that external mass-transfer limitations are negligible. □

We solve the fixed-bed design equation

$$\frac{dN_A}{dV} = R_A = -(1 - \epsilon_B)\eta k c_A$$

between the limits N_{Af} and $0.03N_{Af}$, in which c_A is the A concentration in the fluid. For the first-order, isothermal reaction, the Thiele modulus is independent of A concentration, and is therefore independent of axial position in the bed

$$\Phi = \frac{R}{3} \sqrt{\frac{k}{D_A}} = \frac{0.3\text{cm}}{3} \sqrt{\frac{2.6\text{s}^{-1}}{0.007\text{cm}^2/\text{s}}} = 1.93$$

The effectiveness factor is also therefore a constant

$$\eta = \frac{1}{\Phi} \left[\frac{1}{\tanh 3\Phi} - \frac{1}{3\Phi} \right] = \frac{1}{1.93} \left[1 - \frac{1}{5.78} \right] = 0.429$$

We express the concentration of A in terms of molar flows for an ideal-gas mixture

$$c_A = \frac{P}{RT} \left(\frac{N_A}{N_A + N_B} \right)$$

Solution II

The total molar flow is constant due to the reaction stoichiometry so $N_A + N_B = N_{Af}$ and we have

$$c_A = \frac{P}{RT} \frac{N_A}{N_{Af}}$$

Substituting these values into the material balance, rearranging and integrating over the volume gives

$$V_R = -(1 - \epsilon_B) \left(\frac{RTN_{Af}}{\eta k P} \right) \int_{N_{Af}}^{0.03N_{Af}} \frac{dN_A}{N_A}$$
$$V_R = - \left(\frac{0.6}{0.85} \right) \frac{(82.06)(450)(12)}{(0.429)(2.6)(1.5)} \ln(0.03) = 1.32 \times 10^6 \text{ cm}^3$$

and

$$W_c = \rho_B V_R = \frac{0.6}{1000} (1.32 \times 10^6) = 789 \text{ kg}$$

We see from this example that if the Thiele modulus and effectiveness factors are constant, finding the size of a fixed-bed reactor is no more difficult than finding the size of a plug-flow reactor.

Example 7.4: Mass-transfer limitations in a fixed-bed reactor

Reconsider Example 7.3 given the following two values of the mass-transfer coefficient

$$k_{m1} = 0.07 \text{ cm/s}$$

$$k_{m2} = 1.4 \text{ cm/s}$$



First we calculate the Biot numbers from Equation 7.55 and obtain

$$B_1 = \frac{(0.07)(0.1)}{(0.007)} = 1$$
$$B_2 = \frac{(1.4)(0.1)}{(0.007)} = 20$$

Inspection of Figure 7.17 indicates that we expect a significant reduction in the effectiveness factor due to mass-transfer resistance in the first case, and little effect in the second case. Evaluating the effectiveness factors with Equation 7.58 indeed shows

$$\eta_1 = 0.165$$

$$\eta_2 = 0.397$$

which we can compare to $\eta = 0.429$ from the previous example with no mass-transfer resistance. We can then easily calculate the required catalyst mass from the solution of

the previous example without mass-transfer limitations, and the new values of the effectiveness factors

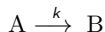
$$V_{R1} = \left(\frac{0.429}{0.165} \right) (789) = 2051 \text{ kg}$$

$$V_{R2} = \left(\frac{0.429}{0.397} \right) (789) = 852 \text{ kg}$$

As we can see, the first mass-transfer coefficient is so small that more than twice as much catalyst is required to achieve the desired conversion compared to the case without mass-transfer limitations. The second mass-transfer coefficient is large enough that only 8% more catalyst is required.

Example 7.5: Second-order, isothermal fixed-bed reactor

Estimate the mass of catalyst required in an isothermal fixed-bed reactor for the second-order, heterogeneous reaction.



$$r = kc_A^2 \quad k = 2.25 \times 10^5 \text{ cm}^3/\text{mol s}$$

The gas feed consists of A and an inert, each with molar flowrate of 10 mol/s, the total pressure is 4.0 atm and the temperature is 550 K. The desired conversion of A is 75%. The catalyst is a spherical pellet with a radius of 0.45 cm. The pellet density is $\rho_p = 0.68 \text{ g/cm}^3$ and the bed density is $\rho_B = 0.60 \text{ g/cm}^3$. The effective diffusivity of A is $0.008 \text{ cm}^2/\text{s}$ and may be assumed constant. You may assume the fluid and pellet surface concentrations are equal. □

We solve the fixed-bed design equation

$$\begin{aligned}\frac{dN_A}{dV} &= R_A = -(1 - \epsilon_B)\eta k c_A^2 \\ N_A(0) &= N_{Af}\end{aligned}\quad (7.78)$$

between the limits N_{Af} and $0.25N_{Af}$. We again express the concentration of A in terms of the molar flows

$$c_A = \frac{P}{RT} \left(\frac{N_A}{N_A + N_B + N_I} \right)$$

As in the previous example, the total molar flow is constant and we know its value at the entrance to the reactor

$$N_T = N_{Af} + N_{Bf} + N_{If} = 2N_{Af}$$

Therefore,

$$c_A = \frac{P}{RT} \frac{N_A}{2N_{Af}} \quad (7.79)$$

Next we use the definition of Φ for n th-order reactions given in Equation 7.42

$$\Phi = \frac{R}{3} \left[\frac{(n+1)k c_A^{n-1}}{2D_A} \right]^{1/2} = \frac{R}{3} \left[\frac{(n+1)k}{2D_A} \left(\frac{P}{RT} \frac{N_A}{2N_{Af}} \right)^{n-1} \right]^{1/2} \quad (7.80)$$

Substituting in the parameter values gives

$$\Phi = 9.17 \left(\frac{N_A}{2N_{Af}} \right)^{1/2} \quad (7.81)$$

For the second-order reaction, Equation 7.81 shows that Φ varies with the molar flow, which means Φ and η vary along the length of the reactor as N_A decreases. We are asked to estimate the catalyst mass needed to achieve a conversion of A equal to 75%. So for this particular example, Φ decreases from 6.49 to 3.24. As shown in Figure 7.9, we can *approximate* the effectiveness factor for the second-order reaction using the analytical result for the first-order reaction, Equation 7.38,

$$\eta = \frac{1}{\Phi} \left[\frac{1}{\tanh 3\Phi} - \frac{1}{3\Phi} \right] \quad (7.82)$$

Summarizing so far, to compute N_A versus V_R , we solve one differential equation, Equation 7.78, in which we use Equation 7.79 for c_A , and Equations 7.81 and 7.82 for Φ and η . We march in V_R until $N_A = 0.25N_{Af}$. The solution to the differential equation is shown in Figure 7.26.

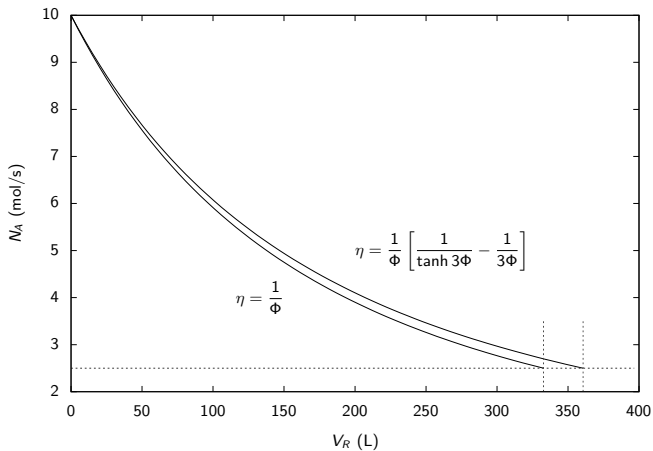


Figure 7.26: Molar flow of A versus reactor volume for second-order, isothermal reaction in a fixed-bed reactor.

The required reactor volume and mass of catalyst are:

$$V_R = 361 \text{ L}, \quad W_c = \rho_B V_R = 216 \text{ kg}$$

As a final exercise, given that Φ ranges from 6.49 to 3.24, we can make the large Φ approximation

$$\eta = \frac{1}{\Phi} \quad (7.83)$$

to obtain a closed-form solution. If we substitute this approximation for η , and Equation 7.80 into Equation 7.78 and rearrange we obtain

$$\frac{dN_A}{dV} = \frac{-(1 - \epsilon_B)\sqrt{k} (P/RT)^{3/2}}{(R/3)\sqrt{3/D_A}(2N_{Af})^{3/2}} N_A^{3/2}$$

Separating and integrating this differential equation gives

$$V_R = \frac{4 \left[(1 - x_A)^{-1/2} - 1 \right] N_{Af} (R/3) \sqrt{3/D_A}}{(1 - \epsilon_B)\sqrt{k} (P/RT)^{3/2}} \quad (7.84)$$

Large Φ approximation

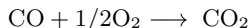
The results for the large Φ approximation also are shown in Figure 7.26. Notice from Figure 7.9 that we are slightly overestimating the value of η using Equation 7.83, so we underestimate the required reactor volume. The reactor size and the percent change in reactor size are

$$V_R = 333 \text{ L}, \quad \Delta = -7.7\%$$

Given that we have a result valid for all Φ that requires solving only a single differential equation, one might question the value of this closed-form solution. One advantage is purely practical. We may not have a computer available. Instructors are usually thinking about in-class examination problems at this juncture. The other important advantage is insight. It is not readily apparent from the differential equation what would happen to the reactor size if we double the pellet size, or halve the rate constant, for example. Equation 7.84, on the other hand, provides the solution's dependence on all parameters. As shown in Figure 7.26 the approximation error is small. Remember to check that the Thiele modulus is large for the entire tube length, however, before using Equation 7.84.

Example 7.6: Hougen-Watson kinetics in a fixed-bed reactor

The following reaction converting CO to CO₂ takes place in a catalytic, fixed-bed reactor operating isothermally at 838 K and 1.0 atm



The following rate expression and parameters are adapted from a different model given by Oh et al. [8]. The rate expression is assumed to be of the Hougen-Watson form

$$r = \frac{k_{\text{CO}} c_{\text{CO}} c_{\text{O}_2}}{1 + K_{\text{CO}}} \quad \text{mol/s cm}^3 \text{ pellet}$$

The constants are provided below

$$k = 1.3828 \times 10^{19} \exp(-13,500/T) \text{ cm}^3/\text{mol s}$$

$$K = 8.099 \times 10^6 \exp(409/T) \text{ cm}^3/\text{mol}$$

$$D_{\text{CO}} = 0.0487 \text{ cm}^2/\text{s}$$

in which T is in Kelvin. The spherical catalyst pellet radius is 0.1 cm, and the densities are $\rho_p = 0.68$, $\rho_B = 0.60 \text{ g/cm}^3$. The feed to the reactor consists of 16.7 mol% CO, 83.3 mol% O₂, and zero CO₂, with volumetric flowrate $Q_f = 792 \text{ L/s}$. Find the reactor volume required to achieve 95% conversion of the CO. □

Solution I

Given the reaction stoichiometry and the excess of O_2 , we can neglect the change in c_{CO_2} and approximate the reaction as pseudo-first order in CO

$$r = \frac{k' c_{CO}}{1 + K_{CO}} \quad \text{mol/s cm}^3 \text{ pellet}$$
$$k' = k c_{O_2 f}$$

which is of the form analyzed in Section 7.4.4. We can write the mass balance for the molar flow of CO,

$$\frac{dN_{CO}}{dV} = -(1 - \epsilon_B) \eta r(c_{CO})$$

in which c_{CO} is the fluid CO concentration. From the reaction stoichiometry, we can express the remaining molar flows in terms of N_{CO}

$$N_{O_2} = N_{O_2 f} + 1/2(N_{CO} - N_{CO f})$$
$$N_{CO_2} = N_{CO f} - N_{CO}$$
$$N = N_{O_2 f} + 1/2(N_{CO} + N_{CO f})$$

The concentrations follow from the molar flows assuming an ideal-gas mixture

$$c_j = \frac{P}{RT} \frac{N_j}{N}$$

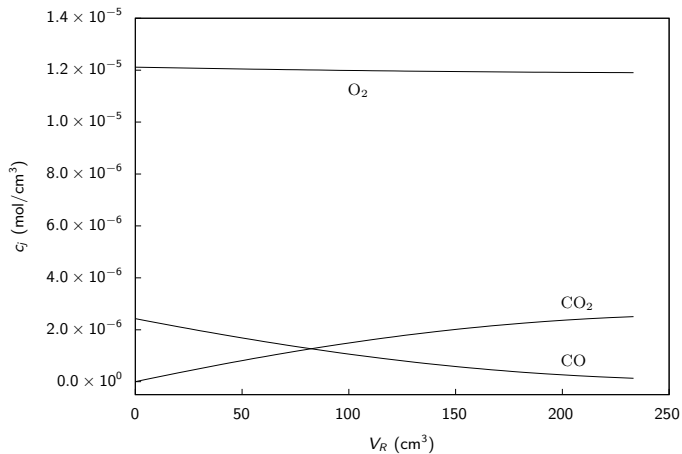


Figure 7.27: Molar concentrations versus reactor volume.

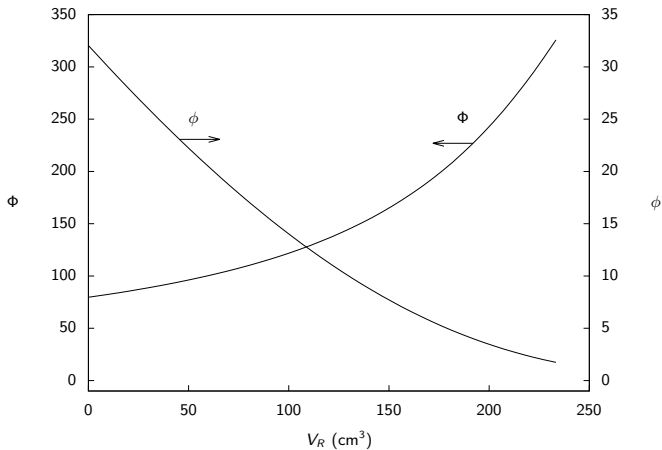


Figure 7.28: Dimensionless equilibrium constant and Thiele modulus versus reactor volume. Values indicate $\eta = 1/\Phi$ is a good approximation for entire reactor.

To decide how to approximate the effectiveness factor shown in Figure 7.14, we evaluate $\phi = K_{CO}CCO$, at the entrance and exit of the fixed-bed reactor. With ϕ evaluated, we compute the Thiele modulus given in Equation 7.52 and obtain

$$\begin{array}{lll} \phi = 32.0 & \Phi = 79.8, & \text{entrance} \\ \phi = 1.74 & \Phi = 326, & \text{exit} \end{array}$$

It is clear from these values and Figure 7.14 that $\eta = 1/\Phi$ is an excellent approximation for this reactor. Substituting this equation for η into the mass balance and solving the differential equation produces the results shown in Figure 7.27. The concentration of O_2 is nearly constant, which justifies the pseudo-first-order rate expression. Reactor volume

$$V_R = 233 \text{ cm}^3$$

is required to achieve 95% conversion of the CO. Recall that the volumetric flowrate varies in this reactor so conversion is based on molar flow, not molar concentration.

Figure 7.28 shows how Φ and ϕ vary with position in the reactor.

In the previous examples, we have exploited the idea of an effectiveness factor to reduce fixed-bed reactor models to the same form as plug-flow reactor models. This approach is useful and solves several important cases, but this approach is also limited and can take us only so far. In the general case, we must contend with multiple reactions that are not first order, nonconstant thermochemical properties, and nonisothermal behavior in the pellet and the fluid. For these cases, we have no alternative but to solve numerically for

the temperature and species concentrations profiles in both the pellet and the bed. As a final example, we compute the numerical solution to a problem of this type. We use the collocation method to solve the next example, which involves five species, two reactions with Hougen-Watson kinetics, both diffusion and external mass-transfer limitations, and nonconstant fluid temperature, pressure and volumetric flowrate.

Example 7.7: Multiple-reaction, nonisothermal fixed-bed reactor

Evaluate the performance of the catalytic converter in converting CO and propylene. Determine the amount of catalyst required to convert 99.6% of the CO and propylene. The reaction chemistry and pellet mass-transfer parameters are given in Table 7.5. The feed conditions and heat-transfer parameters are given in Table 7.6.



Parameter	Value	Units
P_f	2.02×10^5	N/m ²
T_f	550	K
R_t	5.0	cm
u_f	75	cm/s
T_a	325	K
U^o	5.5×10^{-3}	cal/(cm ² Ks)
ΔH_{R1}	-67.63×10^3	cal/(mol CO K)
ΔH_{R2}	-460.4×10^3	cal/(mol C ₃ H ₆ K)
\hat{C}_p	0.25	cal/(g K)
μ_f	0.028×10^{-2}	g/(cm s)
ρ_b	0.51	g/cm ³
ρ_p	0.68	g/cm ³

Table 7.6: Feed flowrate and heat-transfer parameters for the fixed-bed catalytic converter.

- The fluid balances govern the change in the fluid concentrations, temperature and pressure.
- The pellet concentration profiles are solved with the collocation approach.
- The pellet and fluid concentrations are coupled through the mass-transfer boundary condition.
- The fluid concentrations are shown in Figure 7.29.
- A bed volume of 1098 cm^3 is required to convert the CO and C_3H_6 . Figure 7.29 also shows that oxygen is in slight excess.

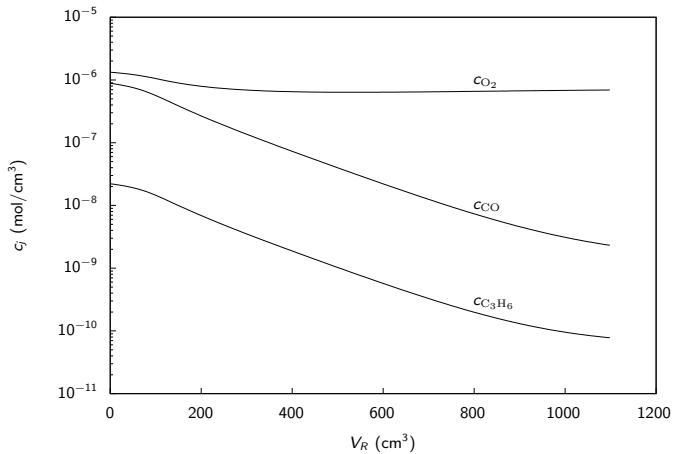


Figure 7.29: Fluid molar concentrations versus reactor volume.

- The reactor temperature and pressure are shown in Figure 7.30. The feed enters at 550 K, and the reactor experiences about a 130 K temperature rise while the reaction essentially completes; the heat losses then reduce the temperature to less than 500 K by the exit.
- The pressure drops from the feed value of 2.0 atm to 1.55 atm at the exit. Notice the catalytic converter exit pressure of 1.55 atm must be large enough to account for the remaining pressure drops in the tail pipe and muffler.

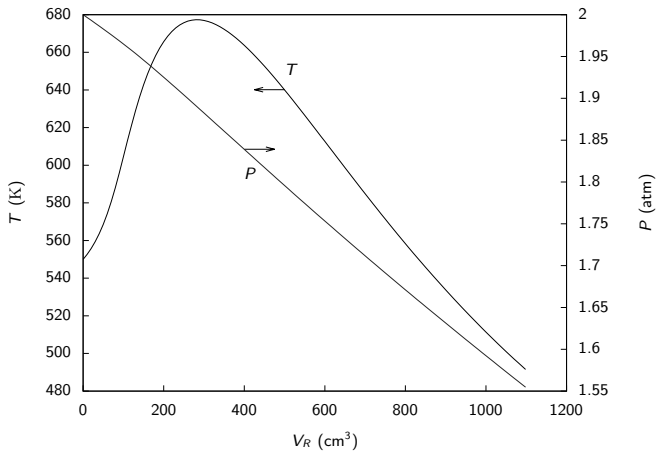


Figure 7.30: Fluid temperature and pressure versus reactor volume.

- In Figures 7.31 and 7.32, the pellet CO concentration profile at several reactor positions is displayed.
- We see that as the reactor heats up, the reaction rates become large and the CO is rapidly converted inside the pellet.
- By 490 cm³ in the reactor, the pellet exterior CO concentration has dropped by two orders of magnitude, and the profile inside the pellet has become very steep.
- As the reactions go to completion and the heat losses cool the reactor, the reaction rates drop. At 890 cm³, the CO begins to diffuse back into the pellet.
- Finally, the profiles become much flatter near the exit of the reactor.

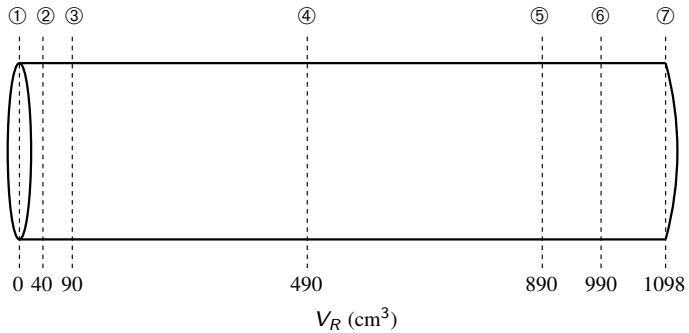


Figure 7.31: Reactor positions for pellet profiles.

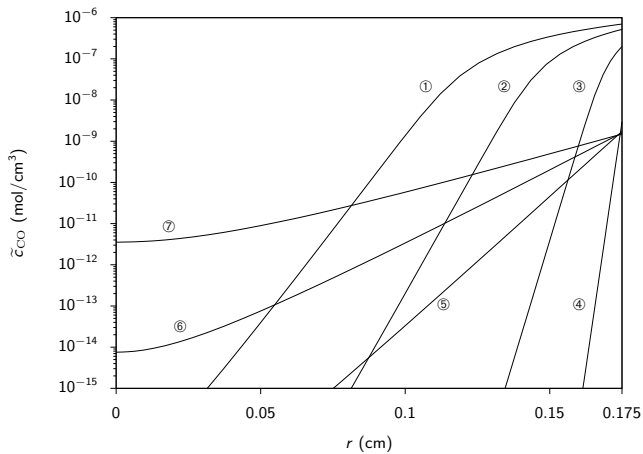


Figure 7.32: Pellet CO profiles at several reactor positions.

- It can be numerically challenging to calculate rapid changes and steep profiles inside the pellet.
- The good news, however, is that accurate pellet profiles are generally *not* required for an accurate calculation of the overall pellet reaction rate. The reason is that when steep profiles are present, essentially all of the reaction occurs in a thin shell near the pellet exterior.
- We can calculate accurately down to concentrations on the order of 10^{-15} as shown in Figure 7.32, and by that point, essentially zero reaction is occurring, and we can calculate an accurate overall pellet reaction rate.
- It is always a good idea to vary the numerical approximation in the pellet profile, by changing the number of collocation points, to ensure convergence in the fluid profiles.
- Congratulations, we have finished the *most difficult example* in the text.

- This chapter treated the fixed-bed reactor, a tubular reactor packed with catalyst pellets.
- We started with a general overview of the transport and reaction events that take place in the fixed-bed reactor: transport by convection in the fluid; diffusion inside the catalyst pores; and adsorption, reaction and desorption on the catalyst surface.
- In order to simplify the model, we assumed an effective diffusivity could be used to describe diffusion in the catalyst particles.
- We next presented the general mass and energy balances for the catalyst particle.

- Next we solved a series of reaction-diffusion problems in a single catalyst particle. These included:
 - Single reaction in an isothermal pellet. This case was further divided into a number of special cases.
 - First-order, irreversible reaction in a spherical particle.
 - Reaction in a semi-infinite slab and cylindrical particle.
 - n th order, irreversible reaction.
 - Hougen-Watson rate expressions.
 - Particle with significant external mass-transfer resistance.
 - Single reaction in a nonisothermal pellet.
 - Multiple reactions.

- For the single-reaction cases, we found a dimensionless number, the Thiele modulus (Φ), which measures the rate of production divided by the rate of diffusion of some component.
- We summarized the production rate using the effectiveness factor (η), the ratio of actual rate to rate evaluated at the pellet exterior surface conditions.
- For the single-reaction, nonisothermal problem, we solved the so-called Weisz-Hicks problem, and determined the temperature and concentration profiles within the pellet. We showed the effectiveness factor can be greater than unity for this case. Multiple steady-state solutions also are possible for this problem.
- For complex reactions involving many species, we must solve numerically the complete reaction-diffusion problem. These problems are challenging because of the steep pellet profiles that are possible.

- Finally, we showed several ways to couple the mass and energy balances over the fluid flowing through a fixed-bed reactor to the balances within the pellet.
- For simple reaction mechanisms, we were still able to use the effectiveness factor approach to solve the fixed-bed reactor problem.
- For complex mechanisms, we solved numerically the full problem given in Equations 7.67–7.77.
- We solved the reaction-diffusion problem in the pellet coupled to the mass and energy balances for the fluid, and we used the Ergun equation to calculate the pressure in the fluid.

Notation I

a	characteristic pellet length, V_p/S_p
A_c	reactor cross-sectional area
B	Biot number for external mass transfer
c	constant for the BET isotherm
c_j	concentration of species j
c_{js}	concentration of species j at the catalyst surface
\bar{c}	dimensionless pellet concentration
\bar{c}_m	total number of active surface sites
D_{AB}	binary diffusion coefficient
D_j	effective diffusion coefficient for species j
D_{jK}	Knudsen diffusion coefficient for species j
D_{jm}	diffusion coefficient for species j in the mixture
D_p	pellet diameter
E_{diff}	activation energy for diffusion
E_{obs}	experimental activation energy
E_{rxn}	intrinsic activation energy for the reaction
ΔH_{Ri}	heat of reaction i
I_j	rate of transport of species j into a pellet
I_0	modified Bessel function of the first kind, zero order
I_1	modified Bessel function of the first kind, first order
k_e	effective thermal conductivity of the pellet

Notation II

k_{mj}	mass-transfer coefficient for species j
k_n	n th-order reaction rate constant
L	pore length
M_j	molecular weight of species j
n_r	number of reactions in the reaction network
N	total molar flow, $\sum_j N_j$
N_j	molar flow of species j
P	pressure
Q	volumetric flowrate
r	radial coordinate in catalyst particle
r_a	average pore radius
r_i	rate of reaction i per unit reactor volume
r_{obs}	observed (or experimental) rate of reaction in the pellet
r_{ip}	total rate of reaction i per unit catalyst volume
\bar{r}	dimensionless radial coordinate
R	spherical pellet radius
R	gas constant
R_j	production rate of species j
R_{jf}	production rate of species j at bulk fluid conditions
R_{jp}	total production rate of species j per unit catalyst volume
R_{js}	production rate of species j at the pellet surface conditions

Notation III

S_g	BET area per gram of catalyst
S_p	external surface area of the catalyst pellet
T	temperature
T_f	bulk fluid temperature
T_s	pellet surface temperature
U^o	overall heat-transfer coefficient
v	volume of gas adsorbed in the BET isotherm
v_m	volume of gas corresponding to an adsorbed monolayer
V	reactor volume coordinate
V_g	pellet void volume per gram of catalyst
V_p	volume of the catalyst pellet
V_R	reactor volume
W_c	total mass of catalyst in the reactor
y_j	mole fraction of species j
z	position coordinate in a slab
ϵ	porosity of the catalyst pellet
ϵ_B	fixed-bed porosity or void fraction
η	effectiveness factor
λ	mean free path
μ_f	bulk fluid density
ν_{ij}	stoichiometric number for the j th species in the i th reaction

ξ	integral of a diffusing species over a bounding surface
ρ	bulk fluid density
ρ_B	reactor bed density
ρ_p	overall catalyst pellet density
ρ_s	catalyst solid-phase density
σ	hard sphere collision radius
τ	tortuosity factor
Φ	Thiele modulus
$\Omega_{D,AB}$	dimensionless function of temperature and the intermolecular potential field for one molecule of A and one molecule of B



R. Aris.

A normalization for the Thiele modulus.
Ind. Eng. Chem. Fundam., 4(2):227–229, 1965.



R. Aris.

The Mathematical Theory of Diffusion and Reaction in Permeable Catalysts. Volume I: The Theory of the Steady State.
Clarendon Press, Oxford, 1975.



R. B. Bird, W. E. Stewart, and E. N. Lightfoot.

Notes on Transport Phenomena.
John Wiley & Sons, New York, 1958.



K. B. Bischoff.

Effectiveness factors for general reaction rate forms.
AIChE J., 11:351, 1965.



S. Brunauer, P. H. Emmett, and E. Teller.

Adsorption of gases in multimolecular layers.
J. Am. Chem. Soc., 60:309–319, 1938.



S. Ergun.

Fluid flow through packed columns.
Chem. Eng. Prog., 48(2):89–94, 1952.



B. C. Gates.

Catalytic Chemistry.
John Wiley & Sons, New York, 1992.



S. H. Oh, J. C. Cavendish, and L. L. Hegedus.

Mathematical modeling of catalytic converter lightoff: Single-pellet studies.
AIChE J., 26(6):935–943, 1980.



C. J. Pereira, J. B. Wang, and A. Varma.

A justification of the internal isothermal model for gas-solid catalytic reactions.
AIChE J., 25(6):1036–1043, 1979.



E. E. Petersen.

A general criterion for diffusion influenced chemical reactions in porous solids.
Chem. Eng. Sci., 20:587–591, 1965.



E. W. Thiele.

Relation between catalytic activity and size of particle.
Ind. Eng. Chem., 31(7):916–920, 1939.



P. B. Weisz.

Zeolites - new horizons in catalysts.
Chem. Tech., 3:498, 1973.



P. B. Weisz and J. S. Hicks.

The behaviour of porous catalyst particles in view of internal mass and heat diffusion effects.
Chem. Eng. Sci., 17:265–275, 1962.